Direct UV-writing of waveguides

Færch, Kjartan Ullitz

Publication date:
2003

Document Version
Publisher's PDF, also known as Version of record

Direct UV-writing of waveguides

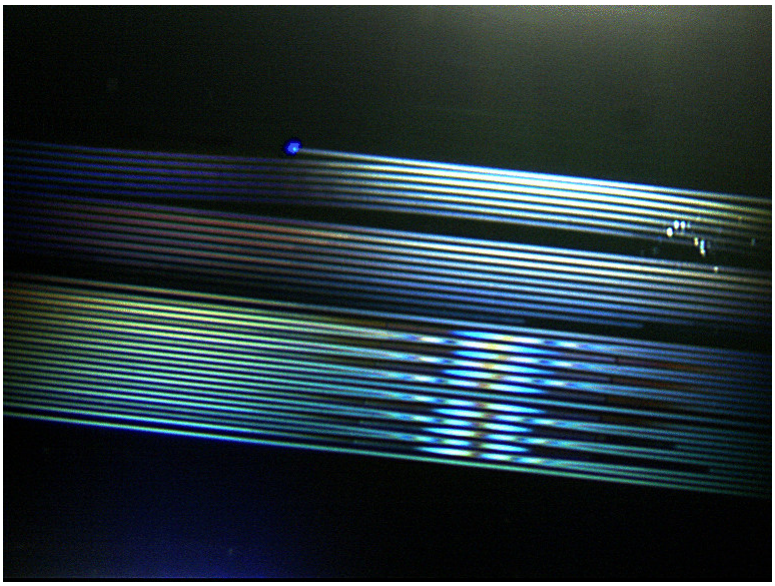

Kjartan Færch

COM Center
Technical University of Denmark
DK-2800 Lyngby

Ph.D. thesis
October 2003

Abstract

The research presented in this Ph.D. thesis is concerned about fabrication of waveguide structures in photosensitized germanosilica thin films by exposure to Ultra-violet (UV) radiation. Using a high pressure loading system and a waveguide fabrication setup, planar waveguiding structures with an UV induced refractive index change of more than 10^{-2} have been obtained. New insight, with respect to understanding the UV induced index change obtained by direct UV writing, has been provided, through experiments conducted with such high-pressure loaded germanosilica samples. This include measurements of the UV induced refractive index change, and spectroscopic measurements of the defect distribution, for various fabrication parameters. A method to measure the concentration of molecular hydrogen in thin film planar waveguide samples is established, and validated for hydrogen loading at up to 12 mole%. The solubility of molecular hydrogen is hereby found not to depend on the loading pressure. Modelling the diffusivity of molecular hydrogen in such samples shows the expected diffusion behavior only when loading at a pressure below 200 bar.

The work has mainly been carried out at the COM Center, Technical University of Denmark, under supervision of Mikael Svalgaard and Martin Kristensen. The work related to luminescence spectroscopy have mainly been carried out at Université de Paris-Sud XI (France) under supervision of Professor B. Poumellec.

Resume

Denne Ph.D. these omhandler fabrikation af bølgeleder strukturer ved en teknik kendt som Direkte UV-skrivning, hvorved en fotofølsom tyndfilm bestående af germanium doteret silica belyses med en fokuseret ultraviolet (UV) laser stråle. Herved kan man inducere en lokal forøgelse af brydnings indekset og således forme bølgeledere ved at translatere filmen under UV strålen.

For at opnå rimelige bølgeleder egenskaber kræves en relativ stor ændring i brydnings indekset, hvilket kun har vist sig muligt for det anvendte tyndfilms materiale hvis det indeholder en mængde molekylær brint. Den inducerede brydnings ændring har således vist sig at være stærkt afhængig af brintkoncentrationen under UV belysningen, hvorfor denne sammenhæng har været et gennemgående tema i afhandlingen.

Rent praktisk er der blevet installeret højtryksudstyr på COM centret som muliggør indiffusion af molekylær brint i silica tyndfilms materialer, i koncentrationer på helt op til 20 mol%. Herved har det været muligt at fremstille bølgeledere med en UV induceret brydnings indeks ændring på over 2×10^{-2}. Der har dog også vist sig en del nye problemer iform af en såkaldt "tærskel effekt", en ikke monoton sammenhæng mellem indeks ændring og brint koncentration, komponent asymmetri og en forøget uddiffusion ved høje koncentrationer.

Mange af disse fænomener er forsøgt belyst i denne these gennem beskrivelser af observationer, eksperimenter og tilhørende måleresultater.

Acknowledgements

First I would like to thank my supervisors Mikael Svalgaard and Martin Kristensen for being very helpful and inspiring during my study. I also wish to thank Bertrand Poumellec and the people working at Laboratoire Physico-Chimie de L'etat Solide, Université de Paris-Sud XI, for the great help during my work in Paris. I have also had a large benefit from working together with Anders Harpøth, Tue Rosbirk, Michael Galili and Marc Andersen in the UV-lab.

I owe thanks to Christian Rosberg, Rasmus Kjær, Mikkel Strange, Clement Lessel and Thomas Nielsen, who has helped me with several smaller projects related to my thesis. The people at NKT integration and Koheras also deserves a big thank for supplying us with samples, equipment and for helping in other practical aspects.

I wish to thank the people in the ILC group: Karin Andersen, Peter Carøe, Karsten Rotwitt, Haiyan Ou, Søren Agger, Jørn Hedegaard, Hugh Philipp and Morten Dyndgaard. Other people that have been of great help are: Jesper B. Jensen, Carl-Johann Marckmann, Henrik Rokkjær, Hans-Jürgen Deyerl, Jacob Fage, Rune Shim.

Frank Persson and Jan Mortensen from the workshop at EMI should also have credit for their support with fabricating small parts for the different setups.

I wish to thank the following people from MIC: Jörg Hübner, Winnie Svendsen, Rasmus Sandberg, Christian Mikkelsen and Ole Hansen.

Finally my wife Louise (and the little guy she is carrying) deserves thanks for the waiting during the long nights of conducting experiments and thesis writing.

Contents

1 Introduction **3**

2 UV-writing setup **7**
2.1 Fabrication setup 7
2.1.1 Components 8
2.1.2 Characteristics 12
2.2 Characterization setup 13

3 UV-written waveguides **17**
3.1 Straight waveguides 17
3.1.1 Hydrogen content 19
3.1.2 UV power and scan velocity 22
3.2 Index asymmetry in UV-written structures 25
3.2.1 Splitter and coupler properties 25
3.2.2 Correcting the induced asymmetry 28

4 UV-induced defects in germanosilica **32**
4.1 Germanosilica structure 35
4.1.1 UV-induced defects 36
4.2 UV-intensity threshold 39
4.2.1 Photo-luminescence measurements 43
4.3 Thermal stability 59
4.3.1 Decay model 61
4.3.2 Experimental 63

5 Molecular hydrogen in silica thin-films **68**
5.1 High pressure loading 71
5.2 Optical properties of loaded samples 73
5.2.1 Optical attenuation 73
5.2.2 Effective index drift 77
5.2.3 Birefringence 79
5.3 Diffusion and solubility in germanosilica 82
5.3.1 Diffusion 83
5.3.2 Solubility 88

6 Conclusion **91**

Chapter 1

Introduction

Fabrication of integrated optical devices, based on planar waveguides, is a highly competitive field of research, involving major universities and corporate institutions throughout Europe, North America and Southeast Asia. The main technology currently used for fabrication of integrated optical waveguide devices is based on photolithography and reactive ion etching, carried out in highly controlled cleanroom facilities. These fabrication techniques requires substantial investments in production facilities and manpower, thereby constituting a significant barrier for the industry.

An alternative fabrication method has previously been demonstrated at DTU, whereby waveguide components are written directly into a planar germanosilica glass sample with a focussed ultraviolet (UV) laser beam [1]. This "Direct UV-writing" method of fabricating optical waveguides eliminates the need for photolithography and etching, hereby simplifying the fabrication process significant and as a consequence reducing the need for expensive cleanroom processing. The method is thus a good alternative to the traditional cleanroom fabrication process of making waveguides.

An integral part of the direct UV-writing process is enhancement of the germanosilica UV photosensitivity, by loading samples with either molecular hydrogen or its deuterium isotope [2]. This loading has previously been done by placing the samples in a chamber pressurized with hydrogen or

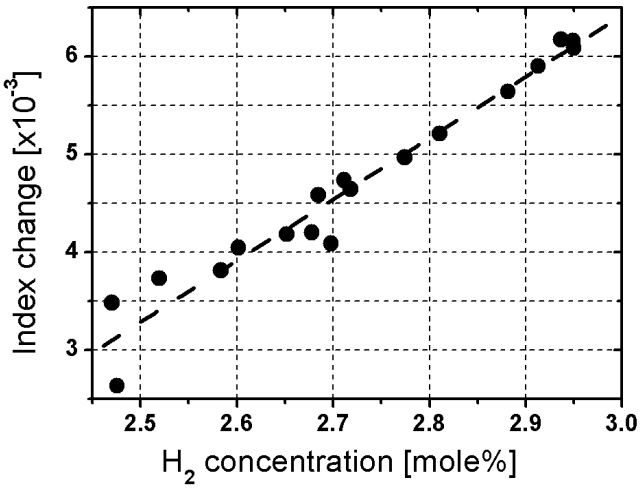

Figure 1-1: UV induced refractive index change obtained with the direct UV writing technique for different amounts of hydrogen dissolved in the sample prior to UV exposure.

deuterium to a pressure of 200 bar. The samples are hereby filled with the diffusing gas to a concentration of up to 3 mole% through a diffusion process. Performing UV-writing in such loaded samples, makes it possible to obtain an UV induced refractive index change of up to 1×10^{-2}. Recent research suggest that significantly larger index changes and substantial improvements in waveguide performance can be achieved, by increasing the loading pressure, as indicated by the measurements shown on figure 1-1. The figure shows the results from an experiment, where UV written waveguides have been fabricated in germanosilica samples containing a different concentration of hydrogen prior to the UV exposure. The dashed line indicate a linear slope for the UV induced refractive index, of around 6×10^{-3} per mole% hydrogen dissolved in the sample, starting at an index value of 3×10^{-3} by 2.45 mole% to more than 6×10^{-3} at 2.95 mole%. There are no indications of the index change process saturating near a concentra-

tion of 3 mole%, hence the motivation for implementing the equipment to load samples to an even higher concentration. For this purpose an ultra-high pressure (UHP) chamber has been installed at Research center COM, which enables us to load samples with hydrogen or deuterium at pressures up to 2000 bar.

The main goal of this Ph.D. study has been to investigate the possibilities and problems related to the fabrication of optical waveguide structures in thin film germanosilica samples by direct UV writing, after loading with hydrogen or deuterium at high pressure. Using high pressure loaded germanosilica thin film samples, waveguides with an UV induced refractive index change of several times 10^{-2} have been fabricated. However, during the waveguide fabrication several unexpected effects have shown up, of which some are considered to be of fundamental interest for the direct UV writing technique. These effects include the existence of an UV intensity threshold, a device asymmetry and an enhanced diffusion of molecular hydogen after high pressure loading, investigated by experiments using Bragg gratings, luminescence and absorption spectroscopy.

Chapter 2 will review the direct UV writing setup, by which buried channel waveguide structures are formed in planar glass samples upon exposure to radiation from a 257 nm frequency doubled argon-ion gas laser. Besides the components included in the UV writing setup, the methods and equipment used for characterization of the fabricated waveguide structures are briefly described.

Chapter 3 deals with the observations from fabricating waveguide structures with the direct UV writing setup. An unexpected step like behavior of the induced refractive index change is presented from experiments of fabricating waveguides, in samples containing various hydrogen concentration. A similar threshold effect is observed during waveguide fabrication using different scanning velocities. Finally, an effect that causes certain integrated optical devices to suffer from an asymmetry is discussed, and a method to correct the asymmetry has been applied.

Chapter 4 is concerned about the results obtained at Lab. Physico-chimie de L'etat solide (Univesité de Paris-Sud XI), from investigation of the observed threshold effect. Photoluminescence spectroscopic measurements have been conducted with both heated and UV irradiated samples, in order to investigate the presence of certain point defects. Defects that are observed to characterize the threshold effect. An experiment of trying to separate the UV induced index change process in two sub-processes, heating and UV exposure respectively, has been performed. From these results it is concluded that heating alone is insufficient for increasing the concentration of the specific germanium related defects. Neither will radiation to a low intensity UV beam be able to increase the concentration of the specific defects, even though the irradiation time is quite long. The thermal stability of waveguides fabricated by direct UV writing is investigated by the use of a previously known electron trap model, showing an energy distribution centered around 2.1 eV. The previous used post-process annealing is hereby verified to result in significantly more stable waveguide components.

Chapter 5 is focussed on the estimation of the hydrogen concentration in planar waveguide samples. A method for direct measuring the concentration of molecular hydrogen in samples with a Bragg grating is investigated and validated for concentrations up to 12 mole%. Using this method the diffusivity and solubility of molecular hydrogen in germanosilica samples is characterized, leading to a simple approximative model for describing diffusion of molecular hydrogen in samples loaded up to 200 bar. The diffusivity is also shown to depend on the loading pressure, while the solubility is shown to be independent on the loading pressure.

Chapter 2

UV-writing setup

This chapter is focussed on the experimental setups used for fabrication and characterization of waveguide structures in germanosilica. Both the fabrication and characterization setup will be described briefly, with respect to components and performance.

The first section describes the components and characteristics of the direct UV writing setup used for waveguide fabrication. Only the most important parts of this setup will be summarized, in the order as being reached by the UV beam propagating in the setup. The setup is optimized for the fabrication of buried channel waveguides in germanosilica samples, will also be used in different configurations to suit other purposes, such as Bragg grating fabrication for instance. The section that follows will describe the characterization setup and some of the methods used to evaluate waveguides and the induced refractive index change.

2.1 Fabrication setup

This section describes the setup, used for fabrication of refractive index structures in germanosilica by UV exposure. In general the setup modifies a monochromatic ultraviolet (UV) laser beam, and focusses it onto a photosensitive germanosilica glass sample. By moving the sample underneath

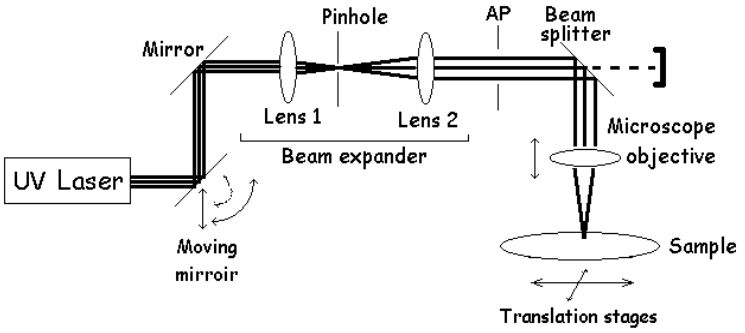

Figure 2-1: Schematic overview of the direct UV writing setup used for fabrication of refractive index structures. The drawing shows the arrangement of the main components such as the laser, lenses, mirrors, apertures and sample.

the focussed beam, waveguiding refractive index structures are formed. A schematic drawing of the setup is shown in figure 2-1.

The success of the writing process is very dependent on the quality of the UV-beam incident on the sample, thus a stable UV source and high grade UV resistant optics are required. Automatized computer control of several components in the setup is important for improving the precision of the beam alignment and maintaining stable operation. The UV-writing setup is placed on an optical table for elimination of vibrations from the floor, and enclosed in a box of polycarbonate sheets with a high efficiency particle absorbing filter mounted above. The filter gives a constant flow of clean air through the setup, that should prevent dust particles from entering the propagating UV beam.

2.1.1 Components

The components in the setup will be described in same order as reached by the propagating UV beam, starting with the UV-source as one of the key components.

The UV source is a frequency doubled argon ion gas laser, lasing at a fundamental wavelength of 514 nm, being frequency doubled to 257 nm by a BBO crystal. In earlier work the argon ion laser was operated at a frequency doubled wavelength of 244 nm [1], but the wavelength of 257 nm have been chosen for the purpose of being able to supply an optical power output of 500 mW (i.e. more than twice as much optical power at a given tube current compared to 244 nm). Even though the overlap with the characteristic 240 nm absorption band for oxygen deficiency centers in germanosilica hereby is reduced, we are able to produce optical waveguides of high quality using less electrical power.

The ideal beam, incident on the samples, would be gaussian shaped, but the actual beam emitted from the laser suffers from aberrations, such as astigmatism, due to limiting apertures in the laser. The astigmatic beam is therefore reshaped and magnified to an Airy like pattern by a beam expander, consisting of two lenses in a 2f configuration with a pinhole positioned in the focal plane between the two lenses. The beam expander has a transmittance of around 40%, and is located close to the focussing microscope objective in order to minimize disturbing effects from air currents.

An aperture, AP, removes the Airy rings from the expanded beam, leaving only the central Airy disc going into the focusing objective. The beam shape of the central Airy disc has a close resemblance to a gaussian shape [3], hence the beam can be considered gaussian shaped in the following.

A beam splitter is used to direct 95% of the remaining power to the focussing objective, while transmitting the remaining 5% into a silicon detector positioned behind the beam splitter. This detector measures the optical power going through the beam expander/aperture, which scales with the power incident onto the sample. By using this detector in combination with a moveable mirror, right after the laser, we are able to realign the beam and keep the incident power fluctuations below 2% during a complete writing process.

After the beamsplitter comes the microscope objective, which has a focal length of 40 mm and is optimized for tight focussing of a monochromatic

Figure 2-2: Cross sectional cut of sample, showing the measured refractive indicies of the silica layers on top of the silicon substrate

UV beam, correcting for spherical aberrations.

The sample substrate is a 5 inch diameter silicon wafer with a thickness of 650 μm. This substrate has been heated to around 1100°C in an oxygen rich atmosphere, whereby a 16.25 μm thick amorphous silicon dioxide (silica) buffer layer of high quality is grown by thermal oxidation (TOX). A germanium and boron doped silica film is then deposited by chemical vapor deposition (CVD), which forms the 5.5 μm thick photosensitive corelayer. Finally comes a boron and phosphorous doped silica cladding (BPSG) of 11.8 μm thickness, deposited by a similar CVD process. The result is a sample structure as shown by the cross sectional cut on figure 2-2, which also shows the refractive indices as given by the fabricant. The sample is annealed at high temperature in order to remove OH groups from the core and cladding layer. This process of fabricating samples have been performed by the NKT company NKT integration A/S, so we have not had opportunity to alter any of these parameters.

The sample is placed on a vacuum chuck, which can be cooled to around -35°C in order to reduce the outdiffusion of deuterium or hydrogen. The diffusion can hereby be reduced by a factor of 50, compared to room temperature (20°C), which is necessary for maintaining a constant photosensitivity during a writing process that can last 12 hours or more [4]. However, for some of the performed experiments a large diffusion rate is desirable, so in

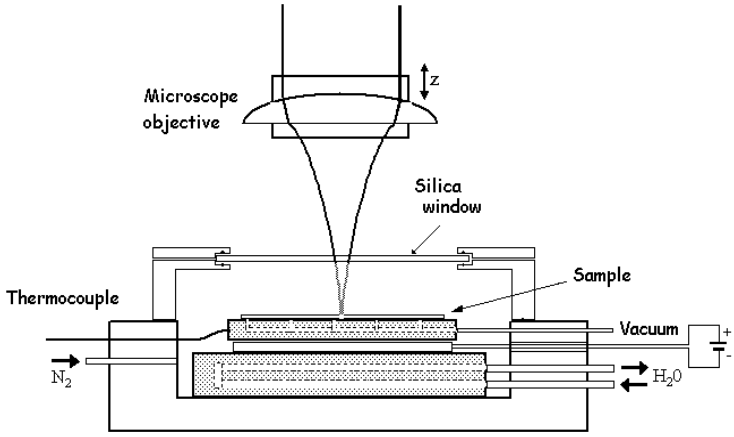

Figure 2-3: Schematic drawing of the sealed chamber, showing the location of several parts such as vacuum chuck, cooling element and water line, thermocouple, nitrogen purge line and sample.

these cases the vacuum chuck can be heated to more than 50°C.

Normally the sample is cooled to -35°C, whereby water vapor will deposit as ice on the sample surface. To avoid this the sample is placed inside a sealed chamber, as shown in figure 2-3, which can be filled with a slight overpressure of nitrogen.

Two high precision DC translation stages (Newport, model PM500) are placed below the chamber, whereby the sample is translated underneath the focussed UV beam in a desired pattern. This enables us to make any structure from straight and circular bended sections, at speeds of several mm/sec with an accuracy of 0.1 μm. The developed structures are typically made from a layout datafile, that supplies a computer with necessary information for controlling the translation stages.

For sample alignment and focussing of the UV beam, a set of video cameras are mounted in the setup, being a Y/C camera and a RGB camera. The RGB camera, mounted to look at the sample inside the chamber with

an incident angle of 45°, is used for monitoring of the focussed UV beam and observations of ice formation. The Y/C camera looks down at the sample at normal incidence, through the beam splitter and microscope objective, and is useful for sample alignment.

2.1.2 Characteristics

The waist of a focussed ideal Gaussian beam is inversely proportional to the beam diameter in front of the focussing lens. The actual beam is described by introducing a M^2-factor [5], which converges against unity for the beam approaching the ideal gaussian shape. The beam waist of such gaussian like beam, passing the focussing objective, is found by the following equation [5]:

$$w_3 = M^2 \frac{\lambda f}{\pi w_2} \tag{2.1}$$

Here f is the focal length of the focussing objective, while w_2 and w_3 are the beam waist radii respectively in front of and after passing the objective. The beam leaving the beam expander is collimated, with a typical beam radius of around 8 mm in front of the focussing objective. The calculated focal spot radius is hereby 1.55 μm ($1/e^2$ intensity) for a measured M^2 value of 1.25. This corresponds well with the measured radius of 1.5 μm from cutting the beam with a razor blade in the focal plane, while monitoring the remaining optical power with a detector as shown on the schematic of figure 2-4. By including the M^2 factor a characteristic Rayleigh length of 24 μm is found, resulting in a focal depth interval of 48 μm, inside which the beam is considered collimated. Having a focal depth comparable to the thickness of the 5.5 μm photosensitive core layer, the beam focussing becomes a critical parameter in the UV writing process. Hence, careful focussing prior to the UV exposure is important to achieve a well defined beam for fabricating waveguide structures.

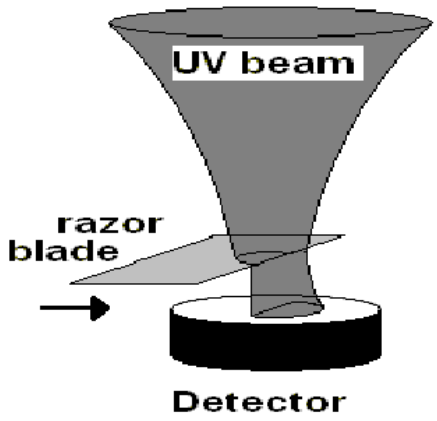

Figure 2-4: Schematic showing the cutting of the UV beam with a razor blade in front of a power detector

2.2 Characterization setup

The characterization setup is used for evaluation of the UV written structures, with respect to physical and optical properties. The width and homogeneity of the fabricated waveguides, is evaluated by visual microscope inspection using an optical Zeiss microscope combined with a high resolution Charge Coupled Device (CCD) camera. The acquired image of a waveguide structure is transferred to a computer, after which the waveguide width is extracted from the images [6].

The insertion loss, polarization dependent loss (PDL) and characterization of the spectral performance is made with an optical fiber setup. With this setup the transmitted or reflected signal can be processed by an optical spectrum analyzer and an EXFO rack. The fibers are butt-coupled to the desired waveguide, after which light is coupled into the structure from a narrow band DFB fiber laser (1557 nm), a broadband whitelight source (800-1800 nm), an ASE source (1520-1570 nm) or a high power

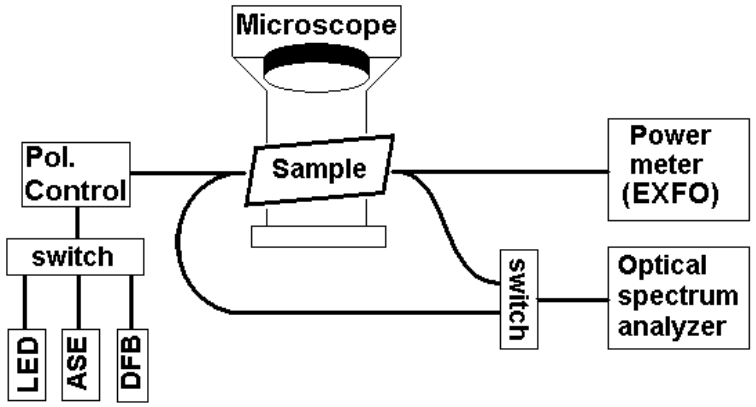

Figure 2-5: Schematic drawing of the characterization setup. Showing the fiber optic setup with light sources, optical switches, polarization controller, sample and analyzers, as well as the microscope used for optical inspection and width measurements.

Light emitting diode (LED) (centered around 1300 nm or 1550 nm). The characterization setup is seen on the schematic of figure 2-5, showing the optical fiber setup components and the microscope.

The EXFO characterization rack consists of a powermeter and a polarization controller, interfaced to a computer which controls the measurements. In addition the optical spectrum analyzer (OSA) can be coupled to the characterization setup, for spectral analysis and monitoring of the transmission or reflection spectrum. Optimal in- and out-coupling of the light in the fabricated waveguide structures is adjusted by moving the optical standard fibers (SMC-28) along 3 orthogonal axes, with precision alignment mounts upon which the cleaved fiber ends are fixed.

For measurements of insertion loss and PDL the DFB laser is coupled into the fiber setup through the EXFO, whereafter a reference loss is obtained by aligning the two fibers ends for maximum transmittance. After this initialization the sample is mounted between the two fibers, which then are aligned for maximum transmittance, by adjusting both alignment

mounts along all axes. This alignment method can produce a reliable insertion loss measurement with an accuracy of +/- 0.1 dB and determine the PDL within +/- 0.06 dB. Due to the optical switches incorporated in the setup the lower limit for PDL measurements is around 0.2 dB. For broadband measurements, light sources can be coupled into the fiber and a transmission- or reflection-spectrum can be acquired with the optical spectrum analyzer.

Weak Bragg gratings have been used intensively for measuring the effective index of the fabricated waveguide structures. The gratings are fabricated by exposing photosensitive waveguides through a phase masks of a given period, Λ_{mask}, whereby the refractive index is modulated with a period of $\Lambda_0 = \frac{\Lambda_{mask}}{2}$. Hence, by measuring the Bragg resonance, λ_{Bragg}, the effective index, n_{eff}, can be extracted according to the Bragg condition [7]:

$$\lambda_{Bragg} = 2n_{eff}\Lambda_0 = n_{eff}\Lambda_{mask} \tag{2.2}$$

From knowledge of the intrinsic refractive index prior to UV exposure, a waveguide mean UV induced refractive index change can be extracted through combining these Bragg resonance measurements with the waveguide width (obtained by visual microscope inspection) and height (given by the photosensitive corelayer thickness). The refractive index extraction is based on approximating the actual complex refractive index profile of the fabricated structures with a simple square shaped step index profile, yielding the same effective index. The approximation has proven its validity for weakly guided UV written waveguide structures after intensive Beam propagation method (BPM) calculations, where the optical properties of the actual measured index profile is compared to simple step index waveguide structures [6]. Using a step index approximation reduces the required processing time considerably, hence this has been the preferred method for evaluating the index of the fabricated structures.

To summarize, this chapter has described the important parts of the

Direct UV-writing setup used for optical waveguide fabrication in planar germanosilica samples. This includes the UV gas laser, the filtering beam expander, the focussing microscope objective, sealed chamber with translation stages and the sample. The characteristics of the 3 μm diameter gaussian shaped UV beam, focussed onto the sample, is shortly described.

The characterization setup and the methods used to characterize the fabricated waveguide structures are described, together with the Bragg condition used to extract the effective index. The BPM based method to extract the refractive index is mentioned. However, for further information about these topics the reader should consult the work of K. Færch [3] and A. Harpøth [6].

Chapter 3

UV-written waveguides

This chapter concerns the characteristics of refractive index waveguiding structures, fabricated in germanosilica samples by UV exposure with the setup described in chapter 2. Here the dependence of the UV induced refractive index change is described with respect to changes in hydrogen concentration, incident UV power or fluence of UV photons. Also problems related to fabrication of waveguides in close proximity to each other will be described based on integrated splitter and coupler structures.

These observations are all based on waveguide fabrication in the germanium doped silica samples described in chapter 2. Before initiating the waveguide fabrication, samples are loaded with several mole percent of hydrogen or deuterium, according to the description of chapter 5. The photosensitivity is hereby enhanced significant [2], which has shown to be essential for waveguide fabrication in such samples [1].

3.1 Straight waveguides

Using the hydrogen loaded germanium doped silica glass samples, straight waveguides have been fabricated using various UV writing parameters. These parameters are mainly the UV-power incident on the sample, the velocity by which samples are translated underneath the UV beam and the

amount of hydrogen or deuterium dissolved in the sample.

The incident UV power is controlled by adjusting the photon emission from the gas laser, while the velocity is adjusted by the commands in the script given to the computer that controls the translation stages. The amount of hydrogen or deuterium contained inside the photosensitive samples is determined through measurements on similar samples, according to chapter 5. Waveguides are then fabricated by translating such samples under the focussed UV beam at velocities around 50 to 1000 μm/s, using an incident UV power of 10-45 mW. After the writing process has ended, the samples are annealed at 80 °C for 24 hours to remove residual hydrogen or deuterium (chapter 4). Finally a weak Bragg grating is inscribed in the waveguide structures (<0.1 dB transmission loss), whereby the effective index can be measured using the setup described in chapter 2.

The optical properties of the fabricated waveguide structures are evaluated through the estimated refractive index, obtained from measurements of the effective index and waveguide width. The waveguides can also be characterized with respect to insertion loss (averaged for all polarization states) and polarization dependent loss (PDL), from butt-coupling standard single mode optical fibers excited with a polarized 1556 nm fiberlaser. The effective index is extracted from the Bragg reflection, during probing with a broadband polarized ASE source. Finally, the waveguide width is measured to an accuracy of +/-1% with a high-resolution optical microscope in combination with a CCD camera.

Previous waveguides have been fabricated in samples loaded with deuterium at a pressure of 190 bar (approx. 3 mole%), using an incident UV power of 45 mW and a scan velocity of 200 μm/s. Such waveguides are around 6.5 μm wide, which is roughly a factor of two larger than the measured UV spot size. Comparing the width to the spotsize suggests that the index change process is saturated in the central part of the exposed area. From mode field calculations using the effective index and measured width we derive a typical index step in the order of 7×10^{-3} for these waveguides. The waveguides are robustly single mode in the 1.5 μm wavelength band

used for optical transmission. The measured insertion loss of such 1 cm long, straight waveguides is 0.4 dB with a PDL of 0.15 dB, which includes both coupling and propagation loss. These values are a little above that of similar waveguides fabricated in a cleanroom.

3.1.1 Hydrogen content

This subsection is focussed on investigating the fabrication of high index buried channel waveguides in germanosilica thin film samples, by the direct UV writing technique. The motivation for doing so is to decrease the size and enhance the functionality of currently fabricated waveguide devices, but also to investigate the process of photosensitivity enhancement in terms of UV induced refractive index change.

As mentioned, previous experiments where based on samples loaded with deuterium at a pressure of 190 bar, hereby giving an equilibrium concentration of upto 3 mole% (chapter 5). Waveguides fabricated in such samples can have a UV induced refractive index step of almost 0.008, as shown by figure 1-1. It is natural to question whether an even higher index change can be obtained simply by increasing the deuterium content. The purpose of our experiment is to investigate the index change process for a wide range of hydrogen concentrations, but instead of loading a large number of samples at different pressures we will rely on the continuous outdiffusion from samples loaded at 1800 bar. For many of these experiment hydrogen loading is used instead of deuterium, but with respect to photosensitivity the effect is believed to be the same. The information obtained through such experiments of outdiffusion can be very useful for determining the usable time interval for fabricating waveguide structures, before the reduced photosensitivity affects the waveguide performance.

Experiment

In the following experiment a number of 10 mm long, straight waveguides are fabricated in identical samples loaded with molecular hydrogen to 20

mole%, using 20 mW of UV power incident on the sample (average intensity 0.3 MW/cm^2) and a translation speed of 200 μm/s. During the writing session the outdiffusion is further accelerated by heating the sample to 51°C, hence only the hydrogen concentration differs during the UV exposure. During the period of UV writing the molecular hydrogen concentration is observed to decrease from 18 mole% down to 8.5 mole%, values which are found from previous diffusion experiments using similar loaded samples with waveguides and Bragg gratings already inscribed according to chapter 5.

After UV processing the sample is annealed at 80°C for 48 hours to remove residual hydrogen and to eliminate defects unstable at room temperature. This is followed by an inscribtion of a weak Bragg grating (transmission loss <1dB) through a phase mask, from which the effective index of each waveguide can be measured. From the measurements of effective index and waveguide width, the UV induced refractive index changes is found for each of the fabricated waveguides. The extracted refractive index change is plotted as a function of the hydrogen concentration during the UV exposure in figure 3-1. The UV induced refractive index step is seen to fluctuate a lot, but exhibits a mean increase from 7×10^{-3} at around 9 mole% to more than 12×10^{-3} at 18 mole%. The mean slope is around 0.59×10^{-3} per mole% hydrogen, as showed by the dashed line. This value can though not be compared directly to the UV induced index increase of 6.2×10^{-3} per mole% obtained at a hydrogen concentration around 3 mole% (figure 1-1), due to the UV intensity in the former case being more than twice as high (UV power of 45 mW). However, figure 3-1 shows a significant difference in the behavior of the UV induced refractive index upon changes in the hydrogen content, which in this case reveals several distinct discontinuous points located at around 12, 14 and 16.5 mole%.

These abrupt changes are also present in the effective index measurements, while the measured width of the fabricated waveguides increases smoothly from 2.0 μm to 3.2 μm over the same range. These step are not caused by the appearance of higher order modes, since none such are ob-

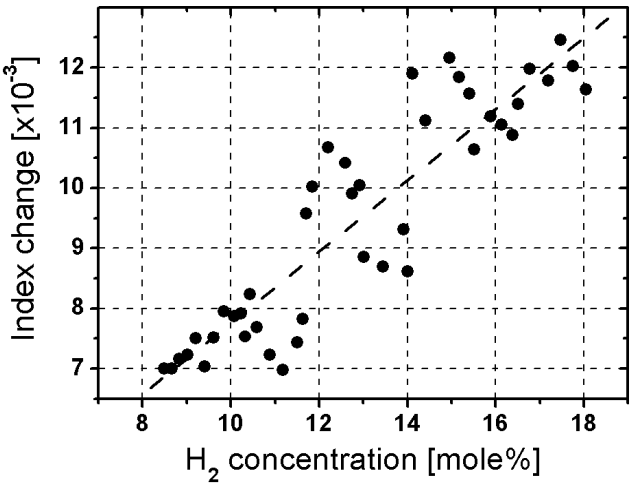

Figure 3-1: Plot of the extracted UV induced refractive index change as a function of hydrogen concentration prior to the UV exposure.

served during the Bragg measurements by any means (excitation of higher order modes is easily achieved by off-axis alignment of the input fiber from the characterization setup). So even if the refractive index extraction should fail for some specific combinations of width and effective index, these discontinuous changes are believed to be a physical effect of the hydrogen concentration reduction. From similar experiments, using 45 mW of UV power and samples only loaded to 3 mole%, no such behavior with abrupt changes has been observed (figure 1-1).

This step-like behavior is interesting from a fundamental point of view, which, to our knowledge, only a newly presented microscopic model have been able to describe [8]. This model assumes that UV excited germanium oxygen deficiency centers (GODC's) are able to transfer the absorbed energy to other specific sites in the surrounding glass matrix. A key parameter controlling this process is the radial density function of the host material,

which, by integration through subsequent shells of neighbors to a germanium center, can cause this step-like behavior. The exact concentration by which these discontinuities occur might change with incident UV power or fluence, which though not have been investigated here.

The effect of these discontinuous points on the technique of direct UV writing is nevertheless that such regions certainly should be avoided in order to achieve a reasonable fabrication yield of high quality optical waveguides. If samples loaded to a concentration close to the observed critical values are used for UV writing, a sudden jump in incident UV power may cause a significant index reduction, which could be devastating for the waveguide performance/reproducibility.

3.1.2 UV power and scan velocity

For hydrogen loaded samples the incident UV intensity is another important parameter during the fabrication of waveguide structures. In fact the UV power might be the parameter that has the largest impact on the obtainable UV induced refractive index change of these samples, next after the concentration of hydrogen [3]. From section 3.1.1 it was shown that, by an incident UV power of 20 mW, the maximum obtainable UV induced refractive index change scales with the hydrogen content. Hence, we believe that loading samples to the largest possible concentration yields the highest refractive index change for a given UV power or fluence [9]. For this reason the following experiments are conducted using samples loaded with hydrogen to the maximum obtainable concentration of around 20 mole%.

Experimental

The experiment described here will reveal the usable range, by which the scan velocity can be varied during waveguide fabrication, for a given UV power of 20 mW. The evaluation criteria will be visual inspection of damage and the obtainable refractive index change, as measured with the characterization setup. For this purpose a series of waveguides are fabricated on the

same sample using scan velocities between 50-900 μm/s. After UV processing the sample is annealed at 80°C for 24 hours, hereby removing residual hydrogen and defects unstable at room temperature. A weak Bragg grating is then inscribed into the waveguides using a phasemask with a period of 1057.09 nm.

The first point of the investigation is visual inspection by microscope, to discover possible UV induced damage inflicted onto the sample. This inspection is necessary as we are only interested in investigating the refractive index growth upon UV exposure, without considering the effects from physical damage of the material. This method gives a rough estimate of the upper limits for the scan velocity applicable for a given UV power, while the lower limit is given by the ability to couple light in and out of the waveguides, or simply to visually identify the presence of a waveguide (partly determined by the microscope NA). For these samples, loaded with hydrogen to 20 mole%, a lower UV power limit of 15 mW and an upper limit of 37 mW was estimated. This is lower than the corresponding UV power of 30 mW and 110 mW found for samples loaded with hydrogen to only 3 mole%. So the increased amount of hydrogen seems to catalyse some of the reactions initiated by the UV exposure.

Extraction of the effective index for each waveguide, according to the measured Bragg resonance and the use of equation 2-2, combined with the measured waveguide width, gives the UV induced refractive index step [6] as seen in figure 3-2. The figure shows the UV induced refractive index change as a function of scan velocity, for waveguides fabricated with 20 mW of incident UV power. Starting at an index step of 16×10^{-3} for a scan velocity of 50 μm/s, the curve decreases almost exponentially towards 11×10^{-3} at a scan velocity of 600 μm/s. At this point the curve seems to exhibit a discontinuity, by suddenly decreasing to indices below 4×10^{-3} for waveguides fabricated with scan velocities above 600 μm/s. This limit, where the index change process seems to be characterized by two different regimes, is referred to as the threshold. The threshold is found at higher scanning velocities for higher UV powers and vice versa. This effect seems

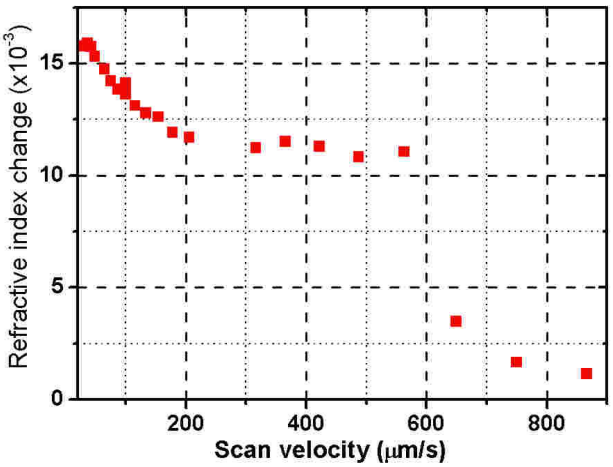

Figure 3-2: UV induced refractive index change obtained as a function of the scanning velocity for an incident power of 20 mW.

to be related both to the incident UV power and the accumulated fluence. It might be that the observed step like behavior, seen in figure 3-1, also is related to this effect. Such an threshold effect is of fundamental importance for understanding the mechanisms behind the UV induced refractive index changes that takes place during direct UV writing, and will therefore be described more detailed in chapter 4.

Further experimental optimization with identical samples has shown that an increase of the incident UV power to 35 mW (0.5 MW/cm^2), can result in a UV induced refractive index change of 0.019 by a hydrogen concentration of 20 mole%. The obtainable UV induced refractive index change seems though to be limited by the UV intensity that the glass is able to withstand, before being clearly damaged. This limit due to damage is found to be around 1 MW/cm^2 for samples loaded with 3 mole% of hydrogen at a given scan velocity, while dropping to just above 0.5 MW/cm^2

for samples loaded with 20 mole%. Due to this damage limit seeming to be dependent on the hydrogen content, further loading to a higher concentration of molecular hydrogen could result in a more narrow interval of usable UV power and hence it might be difficult to obtain damage free waveguides of higher index. It may though be possible to achieve UV induced index changes even larger than the 0.019 reported here, but this will probably require optimization of the sample composition.

3.2 Index asymmetry in UV-written structures

By combining straight and bended waveguide sections, several components have been fabricated, such as Y-branch splitters, directional couplers and Mach-Zender based interferometers. Such UV written structures with waveguides in close proximity have shown to suffer from a refractive index asymmetry, that causes an unexpected distribution of transmitted power between the output arms. Hence, symmetric splitters do not have an even splitting ratio of 50/50, and symmetrical directional couplers are performing as asymmetric directional couplers unable to make 100% cross coupling. This leads to the question: what kind of mechanism can result in two apparently identical waveguides having different refractive indices, after having received the exact same amount of fluence.

This basic problem of UV writing in hydrogen loaded samples will be the topic of the following section, based on experimental observations. A simple but useful method for correcting the observed refractive index asymmetry in such waveguide structures will also be presented, together with a short discussion about the expected origin of the induced refractive index asymmetry.

3.2.1 Splitter and coupler properties

Waveguides in splitter and coupler structures are fabricated according to the description in section 3.1, using an incident UV power of 45 mW and samples loaded with 3 mole% of deuterium. The samples are mounted on

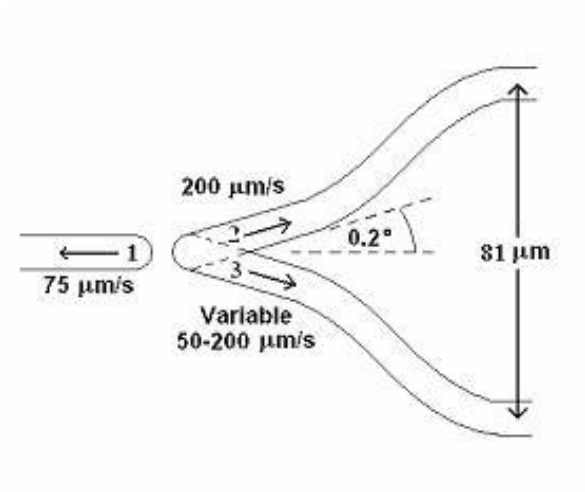

Figure 3-3: Schematic drawing with writing parameters for a fabricated splitter.

the vacuum chuck and thermo-electrically cooled to -35 °C in an nitrogen rich atmosphere.

Starting with a description of a splitter, it consist of three sections: an input arm, a lower output arm and an upper output arm. The sections are scanned sequentially, starting with the input arm, followed by the upper output arm and finally the lower output arm. Each scan starts from a central branching point and moves outwards, as indicated by arrows on the schematic overview in figure 3-3.

Each output arm starts with an 800 μm straight section, tilted at an angle of 0.2° from the input arm, followed by circular arc s-bends (curvature radius of 35 mm). The scan velocity applied for both output arms is 200 μm/s. The output arm spacing is 81 μm and the total device length is roughly 3 mm. Measurements show that the fabricated splitters exhibit a splitting ratio of approximately 0.70 (the relative amount of transmitted power contained in the first written output arm).

The fabricated directional couplers have dual waveguide input/output

ports, connected to a central straight coupling region by s-bends. The scan velocity, radius of curvature and port spacing of the couplers are identical to that of the splitter. The couplers are written in two sequential scans, starting at the same side of the sample, having a center-to-center spacing in the central coupling region of 9 μm. Varying the length of this central coupling region results in the coupling ratio, at 1550 nm wavelength, varying in a squared sinusoidal fashion. This observation confirm that the simple equations for two coupled modes are applicable, with the coupling ratio at 1550 nm peaking for a central coupling region length of 800 μm. However, using a broadband source to measure the cross coupling (i.e. the ratio of power coupled from one port to the opposite) shows a maximum obtainable cross coupling of 0.95, which is below unity as one would expect for a phase matched coupler. Increasing the center-to-center waveguide spacing would increase the maximum obtainable cross coupling ratio towards unity ($>$0.999) as the spacing exceeds 12 μm.

The width of the splitter output waveguides after the branching point where measured to be identical, which was also the case for waveguides in the central coupling region of the coupler. Since both device layouts described are completely symmetrical around the longitudinal axis, the observed asymmetry must be due to a lower refractive index in one of the arms. Observations showed that for the splitter structure it was always the last written output arm that contained the minor fraction of power, hence this waveguide would suffer from a reduced refractive index step. With similar fabrication methods for both splitters and couplers, the induced asymmetry is most likely caused by the same mechanism. From the asymmetric coupler behavior we conclude that the range, over which subsequent scans affect each other, is roughly 12 μm. Simple analysis by beam propagation method (BPM) calculations of the actual splitter and coupler structures, estimates a refractive index difference in the order of a few times 10^{-4} could account for the observed asymmetry.

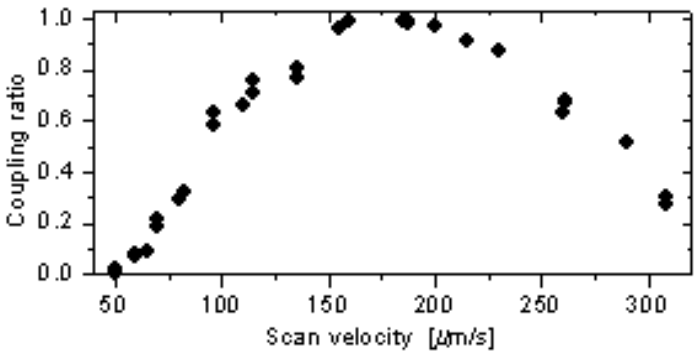

Figure 3-4: Coupling ratio for UV-written couplers as a function of the scan velocity of the second arm, after applying a scan velocity of 200 μm/s for the first arm.

3.2.2 Correcting the induced asymmetry

A non-symmetrical power distribution is undesirable in many situations, such as interferometric applications and 1 to N power splitting. We have therefore applied a simple method for counter balancing the observed asymmetry, based on the experience that the UV induced index change can be controlled by varying the applied scan velocity. Thus, by appropriately lowering the scan velocity for the second output arm, the index of the two closely spaced waveguides can be matched. This method is illustrated in figure 3-4 for couplers with a center-to-center spacing of 9 μm and a coupling region length of 800 μm, by measurements of the maximum cross coupling obtained with a broad band source. With the scan velocity in the first arm being 200 μm/s the scan velocity of the second arm has to be lowered to 175 μm/s to obtain full cross coupling, and thus similar waveguide indicies.

Implementing a similar method during splitter fabrication gave the results as showed in the measurements of figure 3-5, where symmetrical split-

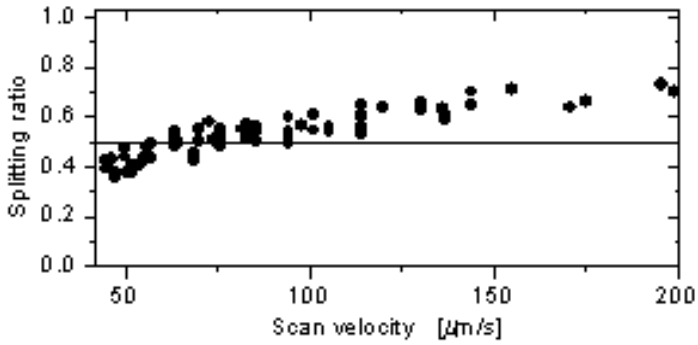

Figure 3-5: Splitting ratio for UV-written splitters as a function of the scan velocity of the second arm, after applying a scan velocity of 200 μm/s for the first arm.

ting is seen to be achieved for a scan velocity in the second arm of around 70 μm/s after using 200 μm/s in the first arm. From effective index measurements on isolated waveguides we have seen that such reductions in scan velocity can result in an index difference of several times 10^{-4}, which is in good agreement with previous estimation of the index asymmetry using BPM calculations. From UV writing sessions over a period of several years we have verified that the optimization described above is quite stable, without need for re-adjustments. In addition, no penalty in terms of higher loss has been observed as a consequence of our asymmetry balancing. Hence, with this method, we are able to reliably fabricate symmetrical couplers and splitters, simply by appropriate adjusting the scan velocity applied during the fabrication of the second arm.

The cause of the observed index asymmetry has been addressed by considering two different scenarios.

The first scenario assumes a halo of UV light surrounding the main spot on the sample, originating from aberrations in the optical system. Waveguides spaced within the extent of this halo are either pre- or post-exposed

to a weak field of UV radiation, depending on the order in which they are written. The observed index asymmetry could then arise from a non-symmetrical response to such pre- or post-exposure. The previous described measurements of the beam intensity profile have shown that the waveguides in the fabricated couplers will experience pre- and post-exposures with UV intensities $< 10^{-3}$ times that experienced in the UV spot center. A series of waveguides were written with either pre- or post-exposure, performed by scanning with a defocussed beam of 10^{-3} times the intensity of the normal UV spot. However, no measurable difference in the effective index ($<3\times10^{-5}$) or width ($<2\%$) was observed in these pre- and post-exposed waveguides. Thus any asymmetry due to pre- or post-exposure only is at least one order of magnitude less than that required to account for the observed device asymmetry.

The second scenario assumes that the high UV intensity of the central beam (approximately 0.6 MW/cm^2) initiates processes in the unexposed glass, as it passes nearby, which reduces the photosensitivity. It is quite difficult to test directly for this scenario, since we are not sure of the nature of the initiated process. However, it is likely that the photosensitivity reduction is coupled to a reduction in the concentration of deuterium, since essentially all of the photosensitivity depends on the presence of deuterium in the sample. To examine the effect of a reduced deuterium concentration, a series of waveguides were written with four-minute intervals, during which deuterium was allowed to outdiffuse at a temperature of 23°C. The deuterium concentration in the core layer at the time of fabrication for each of these waveguides could be determined from the measurements described in chapter 5. Measurements showed that the waveguide width is constant over the sampled range, while the UV induced index decreases almost linearly when lowering the deuterium concentration as shown in figure 1-1. The hereby derived UV induced index step, decrease by roughly 10^{-4} per. percent reduction in the deuterium concentration. A few percent reduction of the deuterium concentration, in the vicinity of the first scan, could easily account for the observed device asymmetry. Such reduction could be

caused by re-distribution of deuterium as it diffuses from the UV spot surroundings into the exposed area, which has been depleted during the index change process. Another cause could be localized outdiffusion through the buffer and cladding near the exposed region. Since the glass is cooled to -35 °C either process requires a thermal heating due to the UV exposure. A 1% deuterium reduction occurring by outdiffusion/re-distribution in the 1/10 seconds it takes the UV spot to pass, would require a temperature increase of several hundred Kelvin. A fact that supports this hypothesis of local heating is that no device asymmetry problems have been experienced to the same degree in non-index matched samples [1], where the UV induced index change depends less strongly on the deuterium content.

In the previous discussion a temperature increase, induced by the high intensity UV beam, is expected to be very important for the UV induced refractive index change in the specific sample material. The temperature increase is expected mainly to originate from a small cubic volume of approximately 200 μm^3, defined by the height of the UV absorbing core layer and the area covered by the width of the scanning UV beam. Measuring the temperature inside such a microscopic part during waveguide fabrication is not trivial, as it is impossible to mechanically probe the temperature without altering it. Probing by vibrational spectroscopy might be possible, but certainly difficult due to the index change process occurring in a limited area

Chapter 4

UV-induced defects in germanosilica

Due to the complexity of the amorphous germanosilica material a large number of models have been proposed for describing the UV induced refractive index change [8][10][11][12]. Still, none of them seems able to give a complete explanation for all observations made during UV processing of germanosilica. The models are typically divided into a group of macroscopic models relating the induced refractive index change to compaction of material, and microscopic models based on electronic transitions in point defects.

Both type of models assume that UV induced changes in the absorption spectrum leads to altering of the refractive index, according to the Kramers-Kronig relation [13]:

$$\Delta n(\lambda) = \frac{1}{2\pi^2} \int_0^\infty \frac{\Delta\alpha(\lambda')d\lambda'}{1-(\lambda'/\lambda)^2} \tag{4.1}$$

This expression relates a change in the absorption spectrum of $\Delta\alpha(\lambda')$, to a refractive index change of Δn at a given wavelength, λ. So for instance a higher absorption in the deep UV can cause an increase of the refractive index at other wavelengths.

This chapter will not investigate if the present waveguide fabrication in these specific hydrogen loaded germanosilica samples can be described by microscopic or macroscopic processes. Instead we will examine a particular threshold effect, that have been observed during direct UV-writing of waveguides in such samples (chapter 3). The investigation is based on photoluminescence spectroscopic measurements, a method often used for analyzing the distribution of electronically excited defect states in silica glass [14][15].

As described in chapter 3, the observed threshold effect causes a sudden drop in the induced refractive index change upon UV exposure of hydrogen loaded germanosilica samples, after reducing the UV intensity below a certain limit. Waveguide structures are only formed if the sample is exposed by sufficient UV intensity over a sufficient amount of time. We believe that this threshold effect is related to the requirement of a certain temperature to be reached inside the UV absorbing corelayer. After reaching this temperature the hydrogen starts to react with the germanosilica, hereby forming germanium related defects that can initiate the index change process upon UV irradiation [16].

Previous experiments of scanning samples at a velocity below the threshold showed that a gradual increase of the scanning velocity would cause a sudden significant decrease of index change [6]. The result of such an experiment with deuterium loaded samples is seen at the image in figure 4-1, which shows a waveguide having been fabricated by increasing the scanning velocity while scanning from left to right. For this specific structure the deuterium content prior to UV writing was around 3 mole%, and the UV power set to around 30 mW. The image shows two different regions, with the point of separation occurring at a scanning velocity around 200 $\mu m/s$ as indicated by the dashed line. The refractive index structure on the right part of the picture is rather weak, while the left side shows a usual waveguide structure. During such experiments the shift was found to happen almost instantaneous, within the order of microseconds, causing a sudden change of the blue luminescence [6]. Hence, we might suspect these two

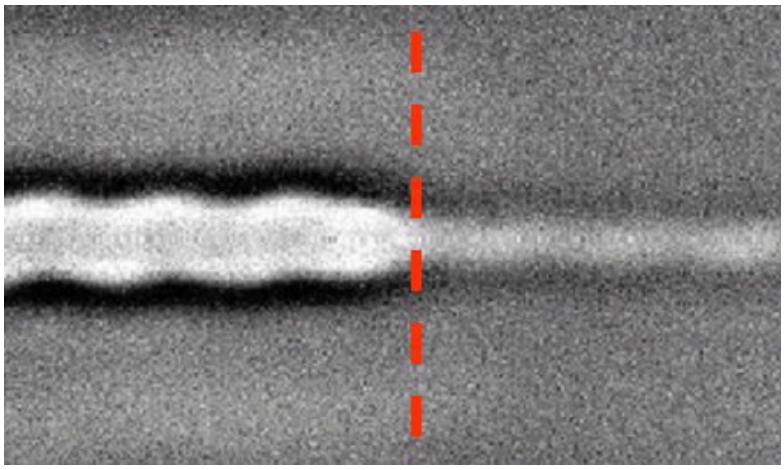

Figure 4-1: Image of a UV written waveguide, showing two different regimes of UV exposure, being separated by a dashed line in the middle. The left side shows a waveguide section exposed with a low scan velocity, while the right side corresponds to a high scan velocity.

regimes are characterized by different defect species. A similar effect of an increased luminescence and index change has been observed by going the otherway of decreasing the scan velocity from above to below threshold.

We believe that the effect described in these observations is equivalent to the situation of fabricating waveguides by exposure of similar samples at an UV intensity above and below the intensity threshold. Investigating this threshold effect is of fundamental interest for understanding the process of refractive index changes induced during UV writing in the specific hydrogen loaded germanosilica samples. Due to the described experiments showing this effect to be accompanied by changes in the blue luminescence, an obvious conclusion would be to investigate the threshold effect on basis of the distribution of luminescent defects.

The following section will describe some defects species, often found in UV irradiated germanosilica. Afterwards comes a section that describes

an experiment related to the above mentioned threshold effect, from sample preparation to luminescence spectroscopic measurements. Finally, the thermal stability of the UV induced refractive index change has been investigated by subjecting fabricated samples to elevated temperatures.

4.1 Germanosilica structure

In pure silica glass the silicon atom is centered in a tetrahedral structure with 4 neighboring oxygen atoms, that each are bonded to two silicon atoms. Even though silica is an amorphous isotropic material, it tends to form ring like structures in a semi-periodic network. The chemical properties of germanium are quite similar to that of silicon, both having 4 valence electrons, thus germanium atoms can substitute for silicon without changing the overall glass structure. Germanosilica is formed by co-doping with a few mole% of germanium during the glass fabrication process, hereby incorporating germanium atoms in the glass network. As these two types of material are much alike, many of the properties observed for silica are also found in germanosilica. Yet, there are dissimilarities that makes germanosilica interesting and widely used in the field of optical waveguides. One of the most important is that the refractive index is slightly higher than that of pure silica, while another is the optical absorption in the UV wavelength range that can give rise to structural or electronic changes upon exposure to UV radiation [17]. The effect of such UV exposure can be an increase of the refractive index, an effect which is used for fabrication of Bragg gratings, post process trimming of optical components and Direct UV writing.

Using germanosilica as the middle corelayer in the specified three layer structure requires a modification of the material composition, due to the intrinsic refractive index otherwise being slightly larger than the surrounding silica buffer and cladding layers. Additional co-doping with boron is used to lower the refractive index of the core layer, and hereby create a homogeneous refractive index distribution through the three layers [18]. The pres-

ence of boron may alter the material properties compared to germanosilica, but for the present study such effects have not been investigated.

4.1.1 UV-induced defects

Several types of defects exist in germanosilica material, as for instance localized network disruptions or wrong bonds. These defects can be caused by post process treatment, but some are also present intrinsically after the material fabrication. In the following we will only describe some of the defects observed in UV-irradiated hydrogen loaded germanosilica.

Defect types

A common defect type is the germanium related oxygen deficient center (GODC), characterized by a germanium atom only bonding to 3 or fewer oxygen atoms [19]. Such defects are often formed during glass deposition in oxygen deficient conditions, and are assumed to play an important role in the UV induced index change process [8]. In this group we have diamagnetic species containing electrons of paired spin, as well as paramagnetic species containing an unpaired electron. The diamagnetic neutral oxygen vacancy (NOV) it is one of the most abundant defect species, characterized by a direct bond, or wrong bond, between germanium and/or silicon atoms [14]. Another diamagnetic defect of interest is the two-fold coordinated germanium atom (Ge^{2+}), bonding to only 2 oxygen atoms. The last oxygen deficient center described is the paramagnetic E'-center, denoting a germanium atom with a single dangling bond. Another common defect type, though not a GODC, is the paramagnetic non-bridging oxygen hole center (NBOHC), which differs from the E'-center by having the dangling bond related to an oxygen atom.

The defect types described here are illustrated in the schematic overview of figure 4-2, showing a simplified germanosilica network with one bond from each silicon or germanium atom hidden. An important property for these defects is the ability to absorb UV photons [14]. With respect to

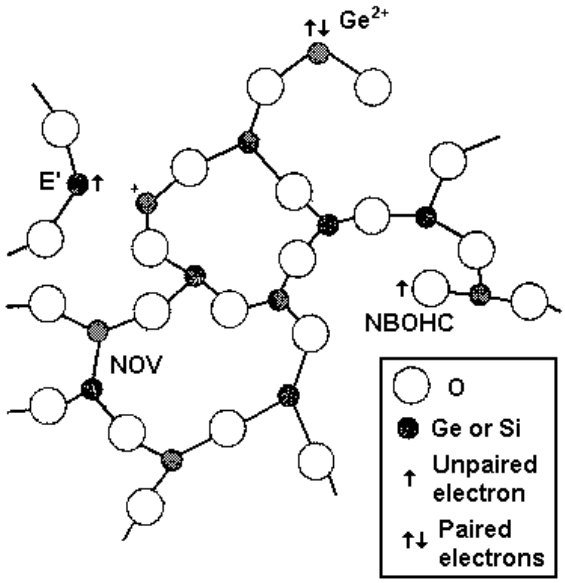

Figure 4-2: Schematic illustration of a simplified germanosilica network, showing some common type of defects

luminescence properties the two-fold coordinated germanium atom is found to emit photons in the UV and visible blue (400 nm) wavelength range [20]. The NBOHC is often related to photon emission in the visible red around 650 nm, while no known emission bands have been observed for the paramagnetic E' center [14]. The width and transition energy of these bands are still subject of several discussions, as is their respective contributions to the process of changing the refractive index upon UV exposure.

Photosensitivity

Several authors suggest that the index change starts when UV radiation interacts with GODC's [8][16], producing different types of defects through reactions that remain unclear. Loading with hydrogen or deuterium is known to enhance the UV photosensitivity significantly [2], which also has

proven very useful for the intrinsically UV insensitive samples used here [4]. The role of molecular hydrogen or deuterium in the UV induced refractive index change process is currently not resolved, except for the fact that the indiffused molecules can enhance the creation of UV absorbing defects species upon reaction with the glass [16][21].

Relating these defects to experiments performed, we note that no measurable blue luminescence have been observed during UV irradiation of virgin unloaded sample. Hence, from the current knowledge we conclude that the GODC concentration is rather low in such untreated samples, consistent with the fact that part of the sample fabrication process involves high temperature annealing in an oxygen rich atmosphere. UV radiation of similar samples, but this time loaded with hydrogen, shows a significant emission of blue luminescence. This is believed to originate from a luminescent center (a two-fold coordinated germanium site), as described in section 4.2.1. Thus we expect GODC's to be formed during this process. A possible reaction scheme could be the following:

$$\equiv \mathrm{Si\text{-}O} \sim \overset{\|}{\mathrm{Ge}} \sim \mathrm{O\text{-}Si} \equiv \; + \mathrm{H_2} \xrightarrow{E} 2 \; \equiv \mathrm{Si\text{-}O\text{-}H} + \; = \mathrm{Ge:}$$

Here the left hand side corresponds to part of a germanosilica lattice and a hydrogen molecule. Upon supplying energy the lattice is somehow broken, resulting in the creation of two OH groups attached to silicon atom and a twofold coordinated Ge^{2+} center. This reaction will mainly occur at germanium sites, due a weaker bonding to oxygen compared to the silicon sites [22]. This reaction is based on the assumption that hydrogen molecules will favour breaking of Ge-O bonds upon rapid heating or dense UV irradiation [21]. The details of how the hydrogen molecule dissociate and the breaking of Ge-O bonds remains unclear, but we expect both thermal and photolytic processes to play an important role [16]. As outlined in the reaction scheme, the product of such an reaction between germanosilica and molecular hydrogen could be formation of a two-fold coordinated germanium defect and two OH groups. Both type of species have been observed in

hydrogen loaded germanosilica samples after UV exposure. Hence, such reaction might be a possible path for the creation of UV absorbing GODC's, that can contribute to the UV induced refractive index change through further reaction mechanisms [21]. The following mechanisms and actual defects responsible for the measured refractive index change will though not be discussed further, as the focus of the described experiments is to investigate the effect that triggers the creation of GODC's in the specific samples.

4.2 UV-intensity threshold

This section describes the experiments and corresponding measurements obtained during investigation of the UV radiation related threshold effect. The idea behind the experiments is to be able to compare samples exposed to UV intensities above and below an observed intensity threshold.

After describing the preparation of samples for the experiments, the measurement setup will be characterized. This is followed by a section describing photoluminescence measurements, by which the samples are investigated, and finally a discussion of the obtained results with respect to tracking differences in defect distributions.

Sample preparation

It is well known that heating a hydrogen loaded optical fiber to several hundred degrees causes the hydrogen to react with the germanium doped core, hereby forming a large amount of hydroxyl (OH) groups [23][24][25]. The creation of OH groups are found to be accompanied by the creation of GODC's in typical optical fibers [16]. Hence, thermally driven reactions between hydrogen and germanosilica can be of central importance for the index change dynamics, especially in the present samples having a low intrinsic photosensitivity. During direct UV-writing such a temperature increase can only be achieved by absorption of UV photons, thus a sufficient flux of UV photons is required in order to reach a specific temperature. If

this condition is met, a substantial degree of hydrogen-glass reaction may occur during the timescale of the UV exposure.

According to the current understanding of the index change process, we will separate this process into separate processes of heating and UV exposure. In practice this is performed by exposing similar samples, loaded with 20 mole% of hydrogen, to different UV intensities, while adjusting the exposure time to yield the same accumulated fluence. We hereby expect samples exposed at a high UV intensity (above threshold) to be subjected to both heating and UV illumination at the same time, while other samples exposed to low intensity UV (below threshold) experience minimal heating. According to previous observations, these two types of treatment should cause a different change in the refractive index, with the high intensity exposed sample obtaining the largest index change. By comparing these two samples we therefore expect to see different defect distributions.

We will also simulate the index change process occuring in high intensity exposed samples, by heating a hydrogen loaded sample to a certain temperature and afterwards expose it to a UV intensity below threshold. Heating with a CO_2 laser was intended [16], but it did not succeed due to technical problems. Instead the hydrogen loaded sample was heated on a hotplate for a few seconds and subsequently UV exposed. However, this does not imply that we are confident that the complete index change process can be separated into independent thermal and photolytic parts, since both processes might are required to take place at the same time in order to obtain a sufficient index change. Figure 4-3 illustrate the different parts of the proposed UV-induced index change process, which the described samples are meant to represent. The figure consist of 3 samples linked by arrows, denoting the proposed reaction paths as described in the following.

The upper solid arrow in figure 4-3 sketches the normal process of changing the refractive index, by exposing a hydrogen loaded sample to a high UV intensity (0.3 MW/cm^2 at 257 nm) with a fluence of approximately 3 kJ/cm^2. This represents the usual method of fabricating waveguides by direct UV writing, and hence this is the process we want to separate. One

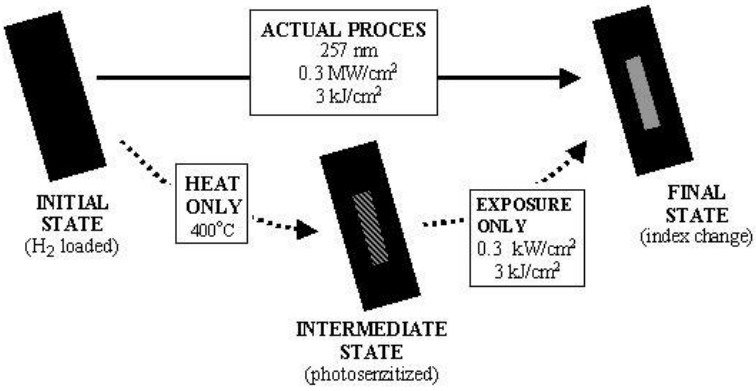

Figure 4-3: Schematic of the different stages during index change, with the actual process described by the solid arrow and the simulated separation in sub-processes denoted by the two dashed arrows.

sample is prepared in this manner. In order to have an exposed area sufficient large for further analysis, closely spaced waveguides are subsequently fabricated over an area of $5 \times 5\ mm^2$ using a scan velocity of 300 $\mu m/s$.

The lower middle part of figure 4-3, denoted by the dashed arrows, sketches the separation of this process into two sub processes of heat (left arrow) and UV-exposure (right arrow). In practice a hydrogen loaded sample is first heated to a temperature of $400°C$, after which it is stored at room temperature for several weeks to ensure removal of residual molecular hydrogen prior to the following UV exposure. The following UV exposure is then performed at a weak intensity of 0.3 kW/cm^2, for a period long enough to achieve the same fluence of 3 kJ/cm^2.

The rapid heating lasted only 4 seconds in order to minimize the destruction of any thermally induced defects [25], performed by placing samples upside down in direct contact with a hot-plate. This is enough time to ensure sufficient heating of the corelayer to the desired temperature $>300°C$. Shorter time intervals could not be used accurately, due to the fact that the sample was placed and removed manually. Heating similar hy-

drogen loaded samples with previously inscribed waveguides to $400°C$ lead to a significant absorption peak at 1400 nm, found by coupling light from a broadband whitelight source through these waveguides. This absorption wavelength corresponds to the expected OH induced absorption band, causing an attenuation of several dB/cm. Annealing experiments (described in section 4.3) with similar samples, though not containing any hydrogen, did not show any measurable attenuation band at 1400 nm upon annealing to $400°C$. Comparing the luminescent intensity of hydrogen loaded and non-loaded samples, both heated to $400°C$, showed an increased amount of blue luminescence from the loaded samples upon illumination by a UV lamp. Hence, these findings confirm that molecular hydrogen may have been thermally activated in germanosilica at temperatures $\sim 400°C$, resulting in generation of OH centers and luminescent GODC's.

Next comes the exposure to weak intensity UV-radiation, performed by defocussing the beam from the UV writing setup to a diameter of approximately 3 mm. The UV intensity is adjusted to yield a 1000 fold reduction from before corresponding to 0.3 kW/cm^2, and consequently there should be no significant UV induced heating of the germanium doped core layer. Waveguides were fabricated by subsequent parallel scanning, while adjusting the scanning velocity to yield a fluence of 3 kJ/cm^2 for the 5×5 mm^2 exposed area. Using the above described method, one sample was prepared by heating and subsequent UV exposure to a weak intensity UV beam, while another sample only was exposed to the weak intensity UV beam.

To summarize we have created 4 different type of samples, corresponding to the different stages in the proposed index change process, as arranged in table 4-1.

Table 4-1

Sample	Condition	Heated	UV intensity	Fluence
Reference	Initial stage	-	-	-
High-UV	Above threshold	-	0.3 MW/cm^2	3 kJ/cm^2
Low-UV	Below threshold	-	0.3 kW/cm^2	3 kJ/cm^2
Heated	Simulated process	$400°C$	0.3 kW/cm^2	3 kJ/cm^2

The untreated (no heat and no UV) "Reference" sample represents the initial state. The "High-UV" sample is only exposed at high-intensity, as by normal waveguide fabrication. The "Low-UV" sample is exposed at an intensity below the threshold, but achieves the same fluence as the High-UV sample. The "Heated" sample is placed on a 400 $°C$ hotplate for four seconds, followed by UV exposure at an intensity below threshold (similar to that of the Low-UV sample).

Probing of the buried germanosilica corelayer with photons should not cause any problem, as long as the sample surfaces are relatively clean and free of scratches. However, as these samples also were intended for electronic probing of the germanium doped core layer, removal of the silica cladding was required due to the sub-micrometer electron penetration depth. So after treating the samples according to the descriptions above (Table 4-1), the 12 μm thick cladding layer was stripped away on all samples using Reactive Ion Etch (RIE). The samples were mounted/glued onto a carrier substrate wafer using photoresist, in order to be able to handle the small samples in the RIE chamber. Using an etching recipe, containing 40 sccm CHF_3 and 8 sccm CF_4 with a plasma ionization power of 300 W, resulted in a measured etch rate of around 0.18 μm/min. Etching each sample for 80 minutes left us halfway down through the core layer, which was verified by microscope inspection of the facet of cleaved samples. This etch processing did not seem to cause any sample contamination. Still, as the germanosilica layer no longer is buried, the possible absorption of moisture from the ambient atmosphere was prevented by placing the samples in a sealed plastic bag along with silicate grains. The encapsulation was broken just prior to conducting the experiments, hereby minimizing a possible absorption of moisture in the meantime.

4.2.1 Photo-luminescence measurements

This section describes the results from conducting photo-luminescence spectroscopic measurements on UV irradiated, heated and non-irradiated ger-

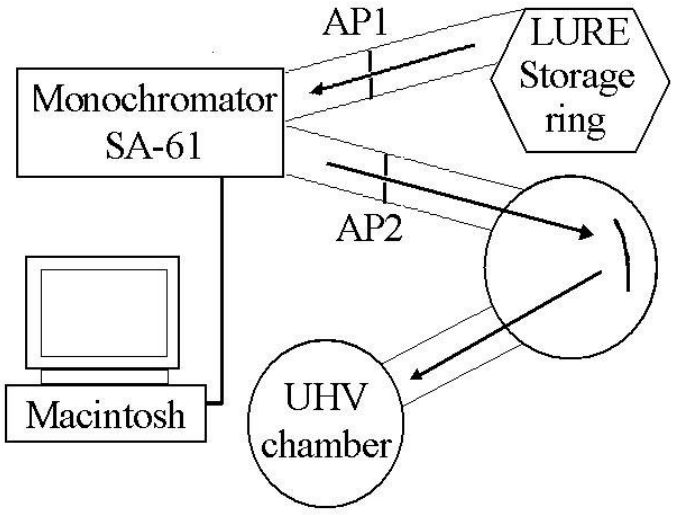

Figure 4-4: Schematic drawing of the setup at beamline SA-61 from the storage ring. The two apertures (AP1 and AP2) are seen together with the computer controlled monochromator, focussing mirror and UHV chamber.

manosilica samples treated according to table 4-1. First the equipment used for the photoluminescence measurements will be characterized, followed by sample analysis using this equipment, and finally a discussion of the obtained results.

Equipment and setup

The measurements are performed using the beamline SA-61 connected to the synchrotron facility LURE (Université de Paris-Sud XI, France). The storage ring contains circulating positrons of 800 MeV kinetic energy, and is able to produce photons within the energy interval from infrared at 1 eV to vacuum ultraviolet (VUV) at around 40 eV. A schematic drawing of the beamline setup, connected to the storage ring, is seen in figure 4-4, showing the storage ring, two apertures, a computer controlled monochromator, a focussing mirror and the ultra high vacuum (UHV) chamber. Radiation

from the storage ring, LURE, is directed by several platinum mirrors (not shown) through the beamshaping input aperture, AP1, and into the 2 m long monochromator. A computer controls the diffraction angle of the monochromator grating, hereby determining the output wavelength of the beam entering the exit aperture, AP 2. The spectral linewidth is less than a nm, as adjusted by the width of this aperture. After passing AP2, a curved mirror focusses the beam onto the samples mounted inside the UHV chamber.

A schematic view of the UHV chamber contents is seen on figure 4-5, with the thick black arrow indicating the reflection from the incoming beam impinging on the samples at an incident angle of 45°. A 50 mm diameter lens captures part of the luminescent emission from the illuminated sample, and focusses the beam on the other side of a quartz window in the chamber wall (shown by the dashed lines). In the outside focal plane one can either place a fiber optic bundle, that guides the luminescent signal to the TRIAX 190 spectrograph from Jobin-Yvon, or place a Hamamatsu R212 UV sensitive photomultiplier tube (PMT). The samples are mounted in the focal plane of the incoming synchrotron beam, on a slider that can be translated in both horizontal and vertical directions. The entire system is evacuated to UHV in order to minimize the presence of foreign molecules. Security valves, located at several positions along the beamline (not shown), can be opened, after which the chamber is directly connected to the storage ring, having platinum mirrors guiding the source light to the samples.

The radiation intensity from the storage ring varies both as a function of wavelength and time. The wavelength response is measured using sodium salicylate powder as a scintillator and a PMT mounted outside the chamber according to figure 4-5. A scintillator is a material of high quantum yield, that converts photons of high energy to a specific energy level measurable to common photodetectors. This is required in order to measure the intensity in the VUV range, where photons otherwise are absorbed by the glass encapsulation of typical PMT's. The emission band of sodium salicylate is found by exposure to VUV radiation from the storage ring, while using

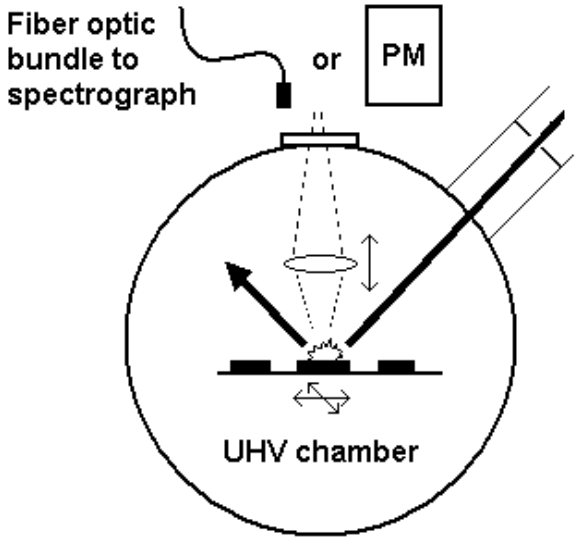

Figure 4-5: Detailed view of the UHV chamber, showing the beam incident on samples mounted on a slider. The collection of luminescence by the lens is focussed outside the chamber (sketched by dashed lines), where either a fiber optic bundle or a photomultiplier is used.

the fiber optic bundle to guide the luminescent photons to the TRIAX spectrograph. The TRIAX 190 spectrograph is capable of resolving UV and visible wavelength spectra with a resolution of 2 nm, by the use of a 600 lines/mm grating and a charge coupled device (CCD) array cooled with liquid nitrogen ($\sim$ 140 K). The sodium salicylate luminescence spectrum is seen in figure 4-6, showing the conversion of high energy photons to an emission band around 3 eV (410 nm). A dashed line indicates the energy limit at 3.5 eV (355 nm), below which sodium salicylate cannot be used as a scintillator due to the incident photon energy overlapping with the emission band. An important property of the sodium salicylate scintillator is the reasonable flat quantum yield throughout the UV-VUV range of interest [26]. Hence, the same amount of luminescent photons are

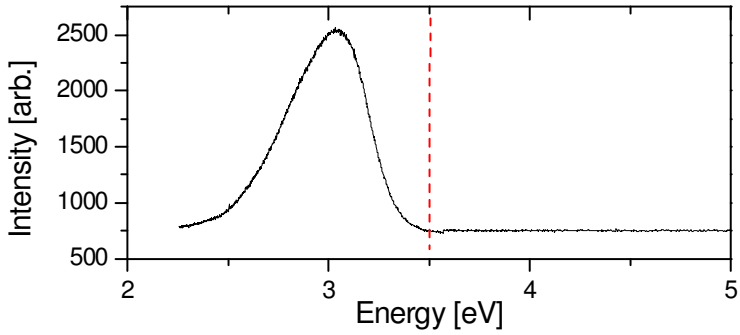

Figure 4-6: Typical luminescence energy spectrum for sodium salicylate, when excited at 180 nm.

emitted for given number of incident photons independent on the excitation wavelength. We also note a background intensity of around 750 in the spectrum of figure 4-6, caused by charge build-up in the CCD array during the 60 seconds of accumulation time. Using sodium salicylate and the PMT, while scanning the excitation energy interval, gives information about the energy distribution of photons passing through beamline SA-61. As the radiation intensity decrease in time along with the loss of positrons in the storage ring, the following formula is used to correct the measured spectra:

$$I_{corr.}(E_{ex}) = \left(\frac{I_{sample}(E_{ex}) - I_{back}(E_{ex})}{I_{salicylate}(E_{ex}) - I_{back}(E_{ex})} \right) \left(\frac{I_{initial}}{I_{actual}} \right) \qquad (4.2)$$

The corrected signal, $I_{corr.}$, is given as a function of the excitation energy, E_{ex}, determined by the monochromator setting. The numerator in the first term on the right hand side contains the measured luminescence signal from the sample, I_{sample}, from which the background, I_{back}, is subtracted. The denominator corresponds to the sodium salicylate signal, $I_{salicylate}$, with background subtraction. A background spectrum was acquired for each measurement, and proper shielding of the TRIAX spectrograph, by a

black carpet, minimized the background signal to a constant value of 750 as seen in figure 4-6. The last term of equation 4.2 corresponds to scaling of the luminescence spectrum with respect to the reduced photon flux. For each measurement the current in the ring, I_{actual}, was monitored, and the spectra scaled according to the initial current, $I_{initial}$, typically around 410 mA. For these measurements we are not interested in absolute values, why the scintillator quantum yield efficiency can be neglected.

The transmission trough the optical collection system may also depend on wavelength. The transmission is measured by replacing one of the samples with a platinum mirror, directing photons from the storage ring directly into the collection system, whereby the transmission is found as a function of wavelength. It is hereby observed that the collection system has a cut-off at 5.5 eV (225 nm), above which a measured signal may degrade due to absorption and possible luminescence from optical components in the system. At energies below this the transmission response was relatively flat in the range of interest, so a constant factor can be used inside this interval to correct for the transmission loss.

Luminescence bands

Having characterized the emission from the storage ring and the optical collection system, the measurements are concentrated around the 4 samples designated Reference, High-UV, Low-UV and Heated according to table 4-1. First the luminescent bands of each sample are revealed by direct exposure to the complete radiation spectrum from the storage ring (broadband excitation) for 1 second. During this exposure the spectrograph collects a luminescent spectrum in an energy interval from 1.3 eV (950 nm) to 6 eV (205 nm).

Figure 4-7 shows the spectra from these 4 samples obtained at 297 K, seen to have emission intensities upto around 1000 counts/second. The dashed curve corresponds to the High-UV sample, the less luminescent dashed/dotted curve to the Low-UV sample, the dotted curve is the Reference, while the somewhat different solid curve is for the Heated sample.

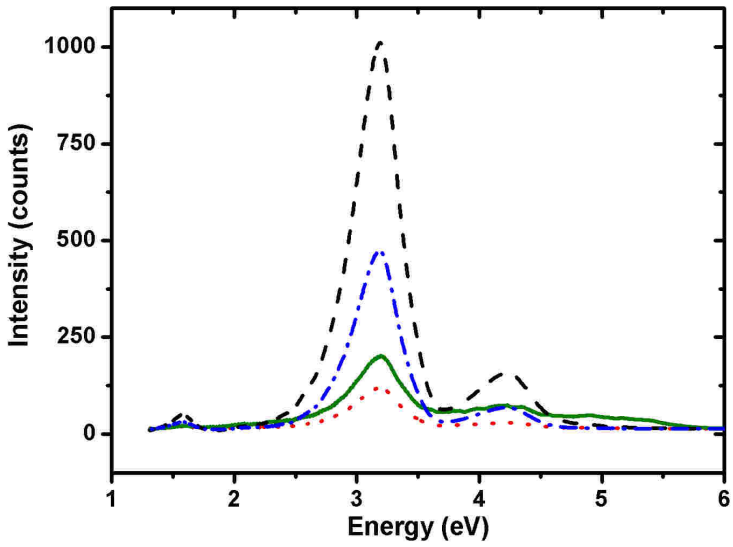

Figure 4-7: Luminescence spectra for the four samples; High-UV(dashed curve), Low-UV(dashed/dotted curve), Reference (dotted curve) and Heated (solid curve) upon broadband excitation.

All samples are seen to emit characteristic luminescence in a strong band centered around 3.2 eV (388 nm) and a weaker band at around 4.25 eV (292 nm). The magnitude of these bands seems to depend on the UV-intensity used during sample fabrication. The spectral shape of the Heated sample is though somewhat different from the others, best described by having a spectrum identical in shape and magnitude to that of the Reference sample plus an additional broadband contribution.

Also seen in figure 4-7 is an additional band peaking at 1.6 eV (780 nm), which is confirmed to be an artifact originating from a higher order diffraction of the 3.2 eV band. The following measurements will therefore concentrate on investigation of the 3.2 and 4.25 eV luminescence bands.

It is important to notice that, apart from the Heated sample, all spectra

seems to have identical shapes. Since the luminescent centers are excited through all possible optical absorption channels within the synchrotron emission spectrum (broadband excitation), the type of defects and their relative concentration in each sample cannot be estimated directly from these measurements alone. For instance one could imagine both UV exposed samples (Low-UV and High-UV) having luminescent centers of identical type and concentration. The luminescent intensity will though still differ, if one sample has a larger concentration of nearby absorption centers, that can lead the absorbed energy to the luminescent centers and hereby excite these [27].

To summarize we have identified the two main luminescent bands, a band of weak emission at 4.25 eV (292 nm) and a band of stronger emission at 3.2 eV (388 nm). Spectra of the two UV-exposed samples and the reference are seen to be of identical shape, while the heated sample seems to have an additional broad emission contribution of unknown width and energy center.

Excitation/emission measurements

The following analysis aims at separating the absorption bands that gives rise to luminescence by measuring an excitation spectrum. In practice the intensity of a given emission band is measured, while varying the excitation wavelength. The excitation linewidth is around 0.02 eV (<1 nm) for these experiments. The luminescent signal obtained by the CCD array is hereby considerably reduced compared to the previous measurements, so the TRIAX is configured to accumulate the collected signal during a 60 second period followed by a correction according to equation 4.2. The result is a set of discrete measurements spaced 0.5 eV apart. These measurements would benefit considerably from the high sensitivity and amplification available with a PMT detector, giving far more and less separated data points. However, due to compatibility problems with the available PMT, and the hardware connected to the synchrotron facility, only the CCD setup could

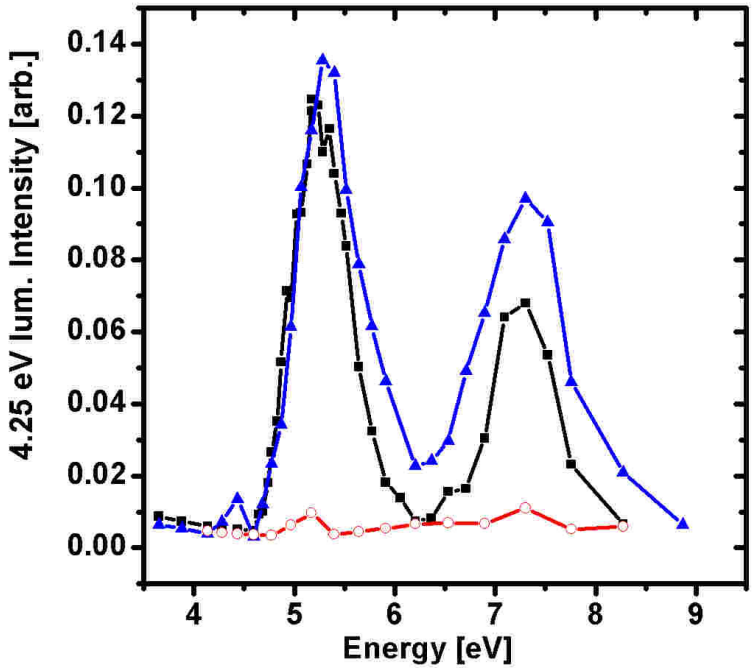

Figure 4-8: Luminescence intensity at 4.25 eV (292 nm) for different excitation energies corresponding to the three samples; High-UV (square markings), Low-UV (triangular markings) and Reference (circular markings).

be used, leading to this restricted number of data points as shown in figure 4-8 and 4-9.

Figure 4-8 shows three spectra for the 4.25 eV (292 nm) luminescence signal, obtained by scanning the excitation energy from 3.5 eV to 9 eV. The square markings correspond to the High-UV exposed sample, the triangular markings to the Low-UV exposed sample and the circular markings to the Reference sample. Decomposition of these spectra into a sum of gaussian [14], is difficult due to the limited amount of data points. However, the spectra of both UV-exposed samples seems to consist of two distinct exci-

tation bands, located at around 5.2 eV (239 nm) and 7.3 eV (170 nm). An additional band located somewhere between 6.5 and 7 eV, seems to induce a slightly asymmetric shape of the 7.3 eV band, but the limited amount of data makes it difficult to verify the exact position of this band. Another small feature around 4.4 eV is neglected, since it most probably originates from scattered excitation light. In overall figure 4-8 seems to be characterized by the dominant gaussian shaped 5.2 eV excitation band, having a measured width of around 0.6-0.7 eV and almost the same magnitude for both UV-exposed samples (Low-UV and High-UV). The 7.3 eV band seems to be somewhat influenced by the weak band located around 6.5-7 eV. With respect to the High-UV sample the intensity of the 7.3 eV band is around 50-60% of the magnitude of the 5.2 eV band. For the Low-UV sample the 6.5-7 eV band intensity seems to have increased slightly, which causes a more asymmetric and broader shaped 7.3 eV band, now having a magnitude of 60-70% compared to the 5.2 eV band. The luminescent intensity of the Reference sample is insufficient for this comparison, still the two characteristic excitation bands at 5.2 and 7.3 eV appear to be present.

The spectra of figure 4-9 corresponds to similar measurements when looking at the 3.2 eV (388 nm) luminescence band with respect to excitation energy. Again, the square markings corresponds to the High-UV sample, the triangular markings to the Low-UV sample and the circular markings to the Reference sample. The overall mean luminescence intensity at 3.2 eV is almost an order of magnitude larger compared to the 4.25 eV luminescence band for most samples. In similarity with the measurements depicted in figure 4-8, the spectrum seems to consist of dominating bands at 5.2 eV and 7.3 eV and a third at around 6.5-7 eV. Once again the magnitude of the 5.2 eV band seems to be equal for both UV exposed samples, still having a width of 0.6-0.7 eV. In contrast to the former measurements the highest luminescent intensity is now around the 7.3 eV excitation band. The 7.3 eV band has almost twice the magnitude compared to the 5.2 eV band for the Low-UV sample, but only 10-20% larger when it comes to the High-UV sample.

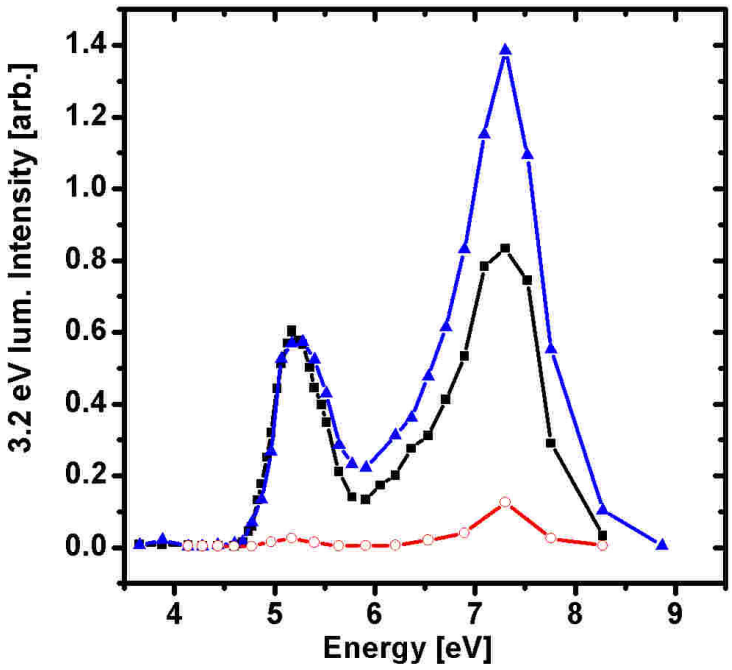

Figure 4-9: Luminescence intensity at 3.2 eV (388 nm) for different excitation energies corresponding to the three samples; High-UV (square markings), Low-UV (triangular markings) and Reference (circular markings).

The above mentioned measurements have all been conducted with the synchrotron facility operating in a 24 packet mode, meaning that the radiation comes in pulses from 24 groups of positrons circulating in the storage ring. With an operation frequency of 4.162 MHz each round trip takes approximately 240.2 ns, giving an average period between pulses of 10 ns. Another possibility is to operate the facility in a 2 packet mode, giving an average period of 120 ns between pulses at the expense of a lower radiation intensity. It is hereby possible to measure luminescence decay, by replacing the CCD array with a UV sensitive high speed photomultiplier (type PMH-100-3). The PMH-100-3 is connected to a single photon counting PC-

module (SPC-430), while the TRIAX monitors the desired luminescence band. Due to the finite time slot of the excitation pulse, the measured luminescence decay is a convolution with the temporal pulse shape, hence the actual luminescent time response can be obtained by iterative fitting [27]. The excitation pulse response was found to be gaussian shaped of $\sim$700 ps FWHM, in agreement with other experiments conducted at the facility. Iterative fitting with the expression of a gaussian shaped pulse convoluted with an exponential decay, gives an approximate decay time for both UV-exposed samples of 4.5 ns with respect to the 4.25 eV luminescence band. The decay time of the 3.2 eV luminescence is much longer than the 120 ns period between excitation pulses, hence we are only able to predict a decay in excess of 20 μs.

To summarize these excitation/emission measurements, we did find coinciding excitation bands for both UV exposed samples (High-UV and Low-UV), located at 5.2 eV (239 nm), 6.5-7 eV (180-190 nm) and 7.3 eV (170 nm). Excitation through these bands causes luminescent emission both at 3.2 eV (388 nm) and 4.25 eV (292 nm), with the intensity of the 3.2 eV band being almost an order of magnitude larger than the the others. These measurements suffer from a limited amount of data points, and only the two UV exposed samples had sufficient luminescent emission for further analysis. Comparison of excitation/emission spectra for these two samples showed equal emission intensities for the 3.2 eV emission band, and also equal intensities for the 4.25 eV band, upon excitation at 5.2 eV. Upon changing excitation energy to 7.3 eV the most intense luminescence for both the 3.2 eV and 4.25 eV bands is observed for the Low-UV sample. Comparison of the overall shape of these spectra indicate that the 4.25 eV luminescence is dominated by excitation at 5.2 eV , while luminescence at 3.2 eV is dominated by excitation around 7.3 eV. The time response for these luminescent centers, upon pulsed excitation, showed a decay time for both UV-exposed samples of around 4.5 ns for the 4.25 eV luminescence band and more than 20 μs for the 3.2 eV luminescence band independent on the excitation energy.

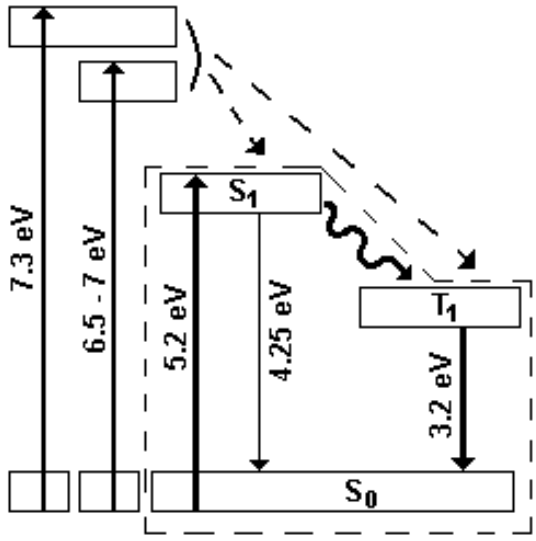

Figure 4-10: Proposed energy band diagram for the performed measurements, showing the system related to the two-fold coordinated germanium center framed by a dashed box. The straight downward pointing arrows indicate radiative transitions, the upward pointing arrow absorption, while the wavelike arrow represent non-radiative intersystem crossing.

Discussion and conclusion

These experiments seems to be in considerable agreement to several others with respect to energy and decay time of the 3.2 and 4.25 eV luminescent bands, as well as the excitation of these through the 5.2 eV band [15][20]. A conclusion is that these bands originate from singlet-singlet and triplet-singlet transitions in the same GODC, being a two fold coordinated Ge^{2+} site (section 4.1). The corresponding band diagram is similar to the one showed inside the dashed box of figure 4-10. Here the straight downward pointing arrows indicate radiative transitions, upward pointing arrows absorption, while the wavelike arrow represent non-radiative inter-

system crossing. The singlet states are denoted S_0 and S_1 and the triplet state T_1. Others report the existence of a weak absorption band at 3.7 eV (335 nm), from a transition between S_0 and T_1. This weak absorption band might also be present in the analyzed samples, but have not been observed during these experiments and this transition therefore not included in figure 4-10. As a consequence of these bands (shown inside the dasahed box of figure 4-10) being observed for all 3 samples (High-UV, Low-UV and Reference), we conclude that the twofold coordinated germanium center (Ge^{2+}) is likely to be present both intrinsically and after UV exposure.

Two additional absorption bands at 6.5-7 eV and 7.3 eV are seen in figure 4-10, corresponding to the remaining two excitation bands observed in figure 4-8 and 4-9. The absolute position of these additional states, as well as the channels relating them to S_1 and T_1 (denoted by dashed arrows in figure 4-10), needs to be verified through further experiments. However, observations of the luminescent emission spectral shape being independent on the excitation energy for both UV-exposed samples could indicate that the luminescent centers are of same type [27] and can be excited through any of the three excitation bands (5.2 eV, 6.5-7eV and 7.3eV). Other experiments with germanosilica samples verified the existence of these additional bands and the relation to the specific luminescent centers through non-radiative intersystem crossing. In addition these excitation bands were ascribed to defects different from those excited at 5.2 eV [15]. This separation is in agreement with our comparison of the two UV exposed samples, showing different emission intensities upon 6.5-7 eV or 7.3 eV excitation, while the 5.2 eV bands seems equal (most obvious in figure 4-9). The two additional excitation channels are therefore separated from the 5.2 eV excited system, framed by the dashed box in figure 4-10. The low emission intensity prevents us from investigating the heated and reference sample in detail. We therefore conclude that the respective defects, responsible for these additional absorption bands, at least are present in UV irradiated samples.

To investigate weather the UV exposed samples differs from each other in magnitude of the 6.5-7 eV and 7.3 eV excitation bands due to absorption

changes or other mechanisms (for instance quenching), would require additional measurements. However, the relative intensity of these two bands seems different upon comparison of excitation/emission spectra for the two UV exposed samples (i.e. different spectral shape between 6-9eV intervals when comparing High-UV and Low-UV samples in figure 4-8 to that of figure4-9). Associating these two bands with different defects would thus seem reasonable.

The conclusion from these observations is that samples exposed to UV intensities above or below threshold (High-UV and Low-UV), do not differ in luminescent intensity with respect to excitation through the 5.2 eV band. This band is found to originate from the twofold coordinated germanium center (section 4.1.1), thus we conclude that the concentration of this GODC type is equal in the two cases. Hence, the present difference in UV intensity, incident on the hydrogen loaded sample during waveguide fabrication, does not have any significant effect on the final concentration of the specific GODC. Correlating these findings to observations of the blue luminescence being more intense during waveguide fabrication with an UV intensity above treshold, lead us to believe that the increased emission is related to something else than a concentration increase of the two-fold coordinated germanium center. This GODC is though still expected to dominate the emission of blue luminescence during waveguide fabrication, since it seems to be the only one having an excitation band that matches the 257 nm photons emitted by the UV laser in the direct writing setup (section 2). This contradiction between an increasing blue luminescence and an identical concentration of the luminescent defect centersfor the two situations (High-UV and Low-UV exposure), might be explained by a temperature difference and hereby also different efficiencies of the non-radiative intersystem crossing between S_1 and T_1 (figure 4-10) [20]. The expected low temperature waveguide fabrication process (Low-UV exposure) causes an intensity reduction of the 3.2 eV luminescence, compared to luminescence from the same band during the high temperature waveguide fabrication process (High-UV exposure). The observations of an increasing blue lu-

minescence as the index change process initiates [6], was performed using equipment unable to distinguish between 3.2 eV and 4.25 eV luminescence. Hence, these observations might show that if the temperature during waveguide fabrication around threshold suddenly is increased, the more efficient 3.2 eV emission band comes to play along with the index change process [20].

We might suspect other differences between these two UV exposed samples, due to the fact that broadband excitation showed the High-UV sample to be more luminescent (figure 4-7). In contrast to this integration of the luminescent intensity, found by narrowband excitation in the interval between 3.5 eV and 9 eV, showed the Low-UV sample to be most luminescent (figure 4-8 and 4-9). A possible explanation for this contradiction could be that the High-UV sample has stronger, shifted or maybe additional absorption bands located at energies outside the 3.5-9 eV interval analyzed here. This would be in agreement with equation 4.1, and observations of samples exposed above the intensity threshold having a larger refractive index. However, such an investigation requires additional measurements outside the excitation interval analyzed here, and knowledge of the absorption spectrum. Especially the latter measurements are rather complicated to interpret for such multi layered silica structures on top of a silicon substrate.

With respect to the sample, both heated and UV exposed (only investigated by broadband excitation), it seems that the magnitude of the luminescence bands at 3.2 eV and 4.25 eV equals that of a reference sample. We suspect that the two-fold coordinated germanium center has not increased in number compared to an untreated reference sample. So, heating to $400°C$ for 4 seconds alone seems not to increase the concentration of Ge^{2+} centers for these samples. Additional experiments of flame brushing similar loaded samples did not show improvement of the photosensitivity during subsequent UV exposure either [28]. From the observed OH concentration increase, not being accompanied by a concentration increase of the two-fold coordinated germanium center, we assume that the reaction

proposed in section 4.1 cannot account for the observations of heated and subsequent UV exposed samples. However, the weak luminescent emission intensity during photo excitation measurements prevented us from resolving the excitation/emission spectrum for the observed broad band luminescence of the heated sample showed in figure 4-7. Thus, investigation of the type of defects created during rapid heating and following weak intensity UV exposure, will have to be based on other methods.

As a consequence, the concentration of two-fold coordinated germanium centers is concluded not to be affected by a decrease in the incident UV intensity of several orders of magnitude during waveguide fabrication, as long as the accumulated fluence is the same. In addition, direct heating to $400°C$ for 4 seconds does not produce a significant increase of this defect type either. Hence, local heating, induced by the high intensity UV beam during direct UV writing, seems not to cause a concentration increase of the specific GODC. However, the resulting UV induced refractive index change is though dependent on the incident UV intensity. So it might be that the UV photons absorbed by such Ge^{2+} centers, created in the initial process, controls a possible following reaction between the hydrogen and sites in the germanosilica corelayer.

4.3 Thermal stability

The topic of this section is thermal annealing of UV written waveguides, that besides being a method for accelerated ageing, can provide us with information about the expected long term behavior.

From previous experiments it is found that UV induced refractive index changes are unstable over time, due to thermal elimination of the induced defects [29]. This effect has previously been investigated for UV induced Bragg gratings in optical fibers, where bleaching causes a degradation of the grating performance. The effect is even more devastating for waveguides fabricated by direct UV writing, as such structures depends entirely on the

UV induced index change. Hence, knowledge of the thermal stability of UV written waveguides is an important aspect.

The thermal stability of UV induced index changes are often investigated using an isothermal annealing process, where the reflectivity and wavelength response of fiber Bragg gratings is measured continuously during heating at elevated temperatures [30]. The measurement technique for planar waveguide structures involves butt-coupling of optical fibers to the sample waveguides, which prevents such continuous measurements of the index during isothermal annealing. A suitable method would therefore be step isochronal annealing, where samples, with previously inscribed waveguides and gratings, are heated at elevated temperatures for a certain amount of time. The sample is cooled down to room temperature between each heating period, during which the UV induced refractive index change is extracted from measurements of the width and Bragg resonance according to chapter 2. The sample is then annealed at an even higher temperature for the same amount of time, before the refractive index is extracted once again. Such a step isochronal annealing experiment can be correlated to isothermal annealing experiments, by a relation between annealing time and temperature given by a parameter known as the demarcation energy [29].

Still there are complications by using such annealing techniques on waveguides fabricated by Direct UV writing, since the waveguide structure could change upon annealing. Thus, measuring the waveguide width is required after each annealing period, while we assume the waveguide height to remain equal to the corelayer thickness for all measurements. The presence of boron in the corelayer could cause additional complications, as it might diffuse out of the corelayer during the high temperature annealing [30]. The effect of boron diffusion would be an increase of the refractive index in the core region, resulting in a different refractive index decay due to this mechanism. Currently we do not have any information on weather such diffusion takes place, so for the present investigation this issue has not been considered.

Returning to our purpose, we have conducted experiments in order to investigate the thermal stability of the UV induced refractive index changes in waveguides fabricated in hydrogen loaded germanosilica samples according to chapter 3. The experiment is based on step isochronal annealing of waveguide samples, after which the refractive index decay is extracted. The first section will shortly review a model that is used to describe the index decay upon thermal annealing, followed by a section describing the experimental results from annealing UV-written waveguides.

4.3.1 Decay model

The thermally induced refractive index decay can be described by a model proposed by Erdogan et. al. [29]. The model is based on observations from annealing experiments with optical fibers, and the assumption that the refractive index decay can be described by depopulation of electron traps, with activation energies distributed according to a state density function $g(E)$ rather than a single energy level.

Figure 4-11 (a) shows a schematic of the proposed model, where UV excited electrons are being trapped in a distribution of energy levels below the conduction band. Here the conduction band corresponds to $E = 0$ and the traps are at energies located $E > 0$ below the conduction band. Assuming a de-trapping of electrons by thermal excitation to depend on temperature, T, and energy depth, E, the mean occupation of states at a time t after UV excitation is given by $f(E,t) = f_0(E)e^{-v_0 t e^{-E/kT}}$ [29]. Where $f_0(E)$ is the initial population of traps immediately after UV excitation, k is the Boltzmann factor and v_0 an attempt frequency. The total number of trapped electrons, $N(t)$, is then given by the expression $N(t) = \int_0^\infty g(E)f(E,t)dE$.

A demarcation energy, E_d, is introduced as the energy level separating populated and depopulated traps, related to temperature and time through the definition $E_d = kT\ln(v_0 t)$. Describing the separation of populated and non-populated traps by such a demarcation energy leads to the following step function approximation; $f(E,t) = f_0(E)$ when $E > E_d$ and $f(E,t) = 0$ for $E < E_d$. Assuming the distribution of traps being much broader than

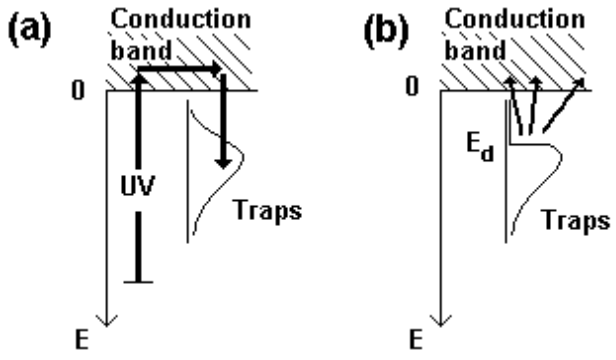

Figure 4-11: Schematic of the distribution and population of traps: (a) The traps are being populated during UV exposure. (b) Traps are being depopulated according to the demarcation energy level.

kT, this step function approximation seems reasonable. The separation of populated and non-populated traps by a demarcation energy is visualized in the simple diagram of figure 4-11 (b), where electrons are released to the conduction band upon thermal excitation. The electron release is assumed to happen for traps at energies below the demarcation energy ($E < E_d$), whereafter these electrons will repopulate the original sites as was before the UV exposure. Using this demarcation energy, the expression for the total number of trapped electrons at a given time can be simplified to:

$$N(t) = \int_{E_d}^{\infty} g(E) f_0(E) dE \tag{4.3}$$

We note that the initial energy distribution of electrons hereby is found as the derivative $\frac{\partial N(t)}{\partial E_d} = -g(E_d)f_0(E_d)$. Hence, assuming a UV induced index change proportional to the total number of trapped electrons, we find the shape of the initial distribution by differentiation of the measured decay curve.

Annealing experiments with standard optical fibers have shown that

the normalized refractive index decay can be approximated well by the expression $\eta(E_d) = \frac{1}{1+e^{(E_d-\Delta E)/kT_0}}$ [29]. The parameters ΔE and T_0 are determined by fitting the expression of $\eta(E_d)$ to the measured data, after which differentiation gives the shape of the initial distribution:

$$g(E)f_0(E) = -\frac{\partial\eta(E)}{\partial E} = \frac{1}{kT_0}\frac{e^{(E-\Delta E)/kT_0}}{\left(1+e^{(E-\Delta E)/kT_0}\right)^2} \tag{4.4}$$

From the definition of the demarcation energy, we get that different sets of temperature and time can yield equivalent demarcation energies according to $kT_1\ln(v_0t_1) = E_d = kT_2\ln(v_0t_2)$. This relation has been verified through experiments, and form the basis of an accelerated ageing process [29]. During accelerated ageing the unstable parts of the UV induced refractive index change are removed by a short period annealing at an elevated temperature. The result of this process is a lowering of the UV induced refractive index change, but with the fabricated components being more stable at normal operating temperature [29].

4.3.2 Experimental

The experiments described in the following are based on UV written waveguides, being annealed at different temperatures between 293 and 973 Kelvin. The waveguides have been fabricated in several germanosilica samples, as specified in chapter 2, loaded with approximately 20 mole% of hydrogen prior to UV exposure. The UV writing parameters are a UV power of 20 mW (0.3 MW/cm^2)and scanning velocities between 30 and 1000 μm$/s$. Afterwards the sample is left at room temperature for several weeks, while residual hydrogen diffuses out of the sample. A Bragg grating is then inscribed in these waveguides, by exposing the samples through a 1071 nm period phase-mask with a pulsed 248 nm excimer laser. This post exposure of the fabricated waveguides may not be optimal, but former experiments showed no significant index change for the fabricated waveguides during such post exposure treatment of unloaded samples (chapter 3).

Prior to the annealing experiments, the UV induced refractive index change was measured, showing values around 3.5×10^{-3} for the weakest waveguides and 16×10^{-3} for the strongest. Each sample is then annealed for 10 hours, after which the refractive index is extracted for several waveguides. The long heating period is used to ensure appropriate sampling of demarcation energies. The same sample is used for several decay measurements, as the refractive index converges towards a state independent of the former treatment [29] (naturally given that the temperature is increased for each annealing step).

However, as mentioned, the use of planar waveguide samples prevents us from performing continuous isochronal annealing (it is not possible to measure while the samples are being annealed), and thus the attempt frequency υ_0 have not been experimentally determined for these waveguides. Instead the demarcation energy of these measurements is based on an attempt frequency of $\upsilon_0 = 10^{14.5} s^{-1}$, obtained from previous experiments with optical fibers [31].

From the measurements of width and effective index a mean UV induced refractive index change is extracted for each waveguide. The result is shown as a function of demarcation energy by solid circles in the plot of figure 4-12. Here the refractive index change for each demarcation energy has been normalized to the initial index change, as measured at a temperature of $23°C$ prior to the annealing experiment (corresponding to a demarcation energy of 1 eV). The error bars denote the standard deviation of the normalized index change, obtained by measuring several waveguides on the same sample after each annealing step, where the different waveguides are fabricated using different scanning velocities. The large deviation above 3 eV is due to difficulties of measuring the effective index in such weak waveguides. However, from the magnitude of these error bars it is clear that all waveguides on a sample will follow the same index decay curve to around 2.5 eV, independent on the scanning velocity used during the waveguide fabrication. The dashed line in figure 4-12 shows a fit to the refractive index change decay from 1.12 eV to 3.25 eV, according to

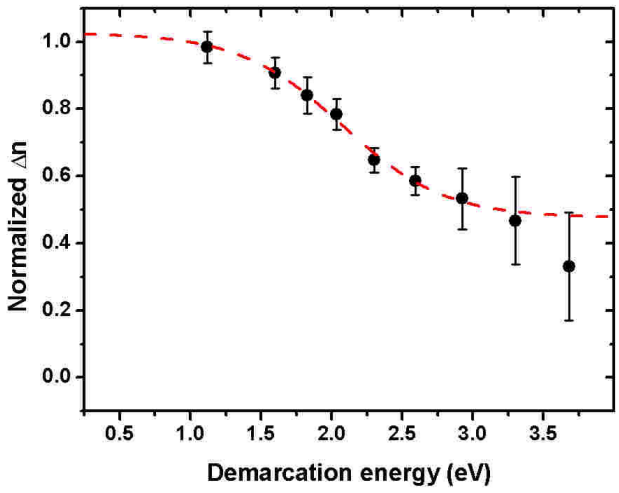

Figure 4-12: Plot of the normalized effective index decay as a function of the demarcation energy. The dashed line shows the fit to the index decay according to the proposed model.

the described model. The fit starts at a normalized index change around 1.03 for a demarcation value of 0.25 eV, and follows the measured effective index decay nicely towards 0.50 at 3.25 eV. The hereby obtained fitting parameters are ΔE = 2.08 eV (+/- 0.05) and a T_0 = 4200 K (+/- 250), with the used demarcation energy of $\upsilon_0 = 10^{14.5} s^{-1}$.

From the derivative of the measured index decay we find the initial distribution of trapped electrons, which in the specific case is related to the range from 0 to 3 eV (equation 4.4), to be well described by a bell shaped curve centered around 2.1 eV with a FWHM of 1.3 eV.

It may seem that the refractive index starts to decrease again for demarcation energies above 3 eV, so one could argue for the existence of an additional distribution of traps at higher demarcation energies [32]. However, at this point the UV written waveguides faints, so it is difficult to

extract the waveguide width, or simply just to measure an effective index. As the only reasonable way to increase the demarcation energy is to anneal at a temperature above $800°C$ we will not benefit from further annealing. If doing so, one could expect diffusion of boron or germanium from the core layer and out into the surrounding layers, which will cause an unknown increase/decrease of the corelayer refractive index along with an index decrease/increase in the surrounding layers [30]. So the index decay for thermal annealing at demarcation energies above 3 eV is currently unknown for direct UV written waveguides.

The starting value for the normalized index change of more than 1 at lower demarcation energies, indicate an initial index change that actually may have been several percent higher than that measured at $23°C$. This is in agreement with the predictions of the index quickly decreasing at $23°C$ within minutes from the time of fabrication [29].

Relating the extracted energy distribution to an operating environment for such UV written waveguides, gives that a decrease in the UV induced refractive index of 6.5 % can be expected after 25 years of operation at $25°C$. To stabilize the UV induced index change, fabricated samples are normally treated at $80°C$ for 24 hours in a post-anneal process. The index hereby decreases by 5.8 %, thus resulting in a decay of only 0.7% during the following 25 years of operation at $23°C$. Hence, the present post-process annealing at $80°C$ stabilizes direct UV written waveguide components considerably.

A distribution of electron traps centered around 2.1 eV is close to the value of 1.9 eV found from experiments with standard optical fibers [33], but far from the values of 1.35 eV and 2.67 eV found in highly germanium doped fibers [32]. However, as the attempt frequency not is experimentally determined, a shift in demarcation energy of the measured index decay can be expected.

Even though the index distribution described might not be observable by luminescence or absorption spectroscopic measurements, monitoring the excitation/emission spectrum during annealing experiments would

certainly be interesting for tracking a possible correlation between the refractive index decay and the observed defect centers.

Another interesting subject is related to the boron diffusion, since it could be that part of the UV induced refractive index change in these samples actually is caused by diffusion of boron out of the waveguide core. Such a process could be initiated by local heating of the core region during direct UV writing of waveguides, which then could be investigated using Secondary Ion Mass Spectroscopy (SIMS) of samples containing a dense distribution of such UV written waveguides.

Chapter 5

Molecular hydrogen in silica thin-films

For the process of fabricating buried channel waveguides by direct UV-writing in the specific germanium doped silica samples, loading with molecular hydrogen or deuterium is essential to enhance the intrinsically low photosensitivity [2]. The UV induced refractive index change depend upon the deuterium content as described in chapter 2. Hence, knowledge of the actual deuterium concentration in the photosensitive core layer prior to UV exposure, is of great interest, not only for direct UV-writing [4], but also for photosensitivity studies in general [2].

The equilibrium concentration is a measure for how much molecular deuterium or hydrogen that can be dissolved in the material at a given loading pressure and temperature. The equilibrium concentration comes from absorption measurements, using silica and germanosilica samples loaded with molecular hydrogen/deuterium at sub-atmospheric pressure [34] [35]. Later experiments validated the expression for calculating the equilibrium concentration when loading at a pressure of 750 bar [2]. However, there is some disagreement about how much molecular hydrogen that actually can be dissolved in silica. Some predict an equilibrium concentration that saturates when above 7-800 bar of loading pressure [36][37], while others

propose a linear pressure dependence that continue to an even higher loading pressure [38][39].

During this study planar samples are loaded with molecular hydrogen at a pressure up to 1800 bar. We will try to determine the equilibrium concentration of molecular hydrogen in such samples after high pressure loading, hereby also investigating the existence of a possible saturation effect. It should be mentioned that even though the experiments are based on loading with molecular hydrogen, the obtained results should in general be applicable for loading with deuterium too.

The hydrogen content is often estimted in optical fibers and bulk samples by absorption- or vibration-spectroscopic techniques. For planar thin-film structures in silica such spectroscopic techniques becomes inappropriate, due to a short interaction length and the layered structure. Another possibility of measuring the hydrogen content originates from experiments with optical fibers loaded at pressures to 100 bar [40], which showed that the effective index varies monotonically along with the hydrogen content dissolved in the light guiding core region of the fiber. A simple and robust method of estimating the concentration of molecular hydrogen in the photosensitive core region, is therefore to measure the effective index drift with a Bragg grating inscribed in the fiber [38].

We will use the same method, of measuring the effective index drift with a Bragg grating, to estimate the hydrogen content in previously fabricated planar germanosilica waveguide structures. The equilibrium concentration will be determined for molecular hydrogen loading up to 1500 bar. However, this requires a validation of the above mentioned Bragg grating method, since former experiments of using this method have been performed with optical fibers loaded at a pressure below 200 bar. So, not only have we increased the loading pressure almost an order of magnitude, the measurements are conducted using planar waveguides instead of optical fibers. The grating method should though be used with caution, since a grating also is sensitive to mechanical changes such as strain. The strain has previously been an unknown parameter in experiments due to the circular structure

of an optical standard fiber [38]. However, in contrast to standard optical fibers, the planar waveguide structure enables us to determine the birefringence, as induced by strain for instance [41]. This actually gives us an additional probe for determination of the hydrogen content in planar samples.

The first part of this chapter will focus on verification of the Bragg grating method, from correlation of the measured molecular hydrogen related absorption with the effective index drift. Starting with a section describing the equipment used for loading of samples with gas phase molecular hydrogen or deuterium. The following section describes the observed modification of the germanosilica optical properties due to the presence of molecular hydrogen, based on measurements of the absorption spectrum and effective index drift in high-pressure loaded samples.

The second part will use the developed Bragg grating method to describe the behavior of molecular hydrogen in high pressure loaded germanosilica samples, with respect to diffusion rate, solubility and determination of the equilibrium concentration.

The experiments described in this chapter uses two different types of samples, both having germanosilica waveguides sandwiched between a silica buffer and cladding layer. The waveguides in sample type 1 are fabricated using the Direct UV writing method, while the waveguides in sample type 2 are fabricated in the cleanroom using photolithography and RIE processing. The important properties of these two types are given in table 5-1, where λ_{Bragg} is the initial Bragg resonance wavelength of an inscribed grating, using a phasemask of period Λ_{mask}.

Table 5-1

Sample	Fabrication	guide length	n_{eff}	Λ_{mask}	λ_{Bragg}
Type 1	UV written	3.5 cm	1.4484	1057.09 nm	1531.06 nm
Type 2	cleanroom	110 cm	1.4559	1065 nm	1550.54 nm

These waveguides are all single-mode at wavelengths above 1400 nm,

and have Bragg gratings inscribed and characterized before being loaded with hydrogen.

5.1 High pressure loading

Prior to most of the following described experiments the specified germanosilica thin film samples have been loaded with molecular hydrogen from gas phase through a diffusion process.

Loading method

The loading method involves placing the samples inside a sealed chamber, which then is pressurized with the diffusing gas for a sufficient time period. The gas molecules will diffuse into the sample, leading to an increase of the gas content towards an equilibrium concentration C_{eq}. This equilibrium concentration is given as the product of solubility S and equilibrium gas pressure P in the surrounding atmosphere, according to the following equation [42]:

$$C_{eq} = SP \tag{5.1}$$

The equilibrium concentration of molecular hydrogen dissolved in standard silica optical fibers have experimentally been determined to 116 ppm/bar at 21°C (1 ppm equals 10^{-6} moles of H_2 per mole of SiO_2) [35]. The equilibrium concentration is temperature dependent with a proportionality factor of $\exp \frac{8.67kJ/mole}{RT}$, with R being the gas constant ($R = \frac{8.31J/mole}{K}$) and T the absolute temperature in Kelvin.

The time required for loading to a certain concentration is usually found from a simple one dimensional fickian diffusion equation [40]. For these planar samples an assumption of hydrogen molecules only diffusing into the thin film from the air/silica surface will lead to a characteristic time, for a hydrogen molecule to diffuse the distance L into the material, given by $t = \frac{L^2}{4D_{H_2}}$. Here we will use a diffusivity for molecular hydrogen in

silica at room temperature (20°C) given by $D_{H_2} = 1.5 \times 10^{-11}\ cm^2/s$ [43], and a corresponding diffusivity of deuterium of $D_{D_2} = 1.4 \times 10^{-11}\ cm^2/s$ [44]. In the following the diffusivity and solubility is considered as being indifferent when comparing silica to germanosilica, due to similar structural- and chemical-properties. As a result the time required to obtain 95% of the equilibrium concentration in a 30 μm thick glass layer is around 120 hours (5 days) of diffusion [1], a calculation based on the assumption that the diffusivity is equal for the three glass layers (cladding, core and buffer). In reality the diffusion time will most likely be shorter due to the hydrogen diffusing into the thin film from both sides. A slight modification of the expression to match circular structures gives a corresponding loading time for a 125 μm diameter optical standard fiber of around 13 days.

Loading equipment

Molecular hydrogen or deuterium is supplied to the chamber from a booster pump, which compresses the gas from a standard gas bottle of maximum 200 bar pressure. This setup is sketched on figure 5-1, where the gas bottle to the left is connected to the booster pump, supplying the chamber with the diffusing gas. The booster pump is capable of pressurizing the chamber with up to 16 times the pressure from the gas bottle, whereby samples can be loaded with molecular hydrogen or deuterium at any pressure up to 2000 bar. This maximum pressure of 2000 bar is due to the structural limit of the loading system, of which the loading chamber and hydraulic control system is seen in the photograph of figure 5-2. Such loading system, with a booster pump, represents a major improvement compared to standard loading equipment, where the obtainable chamber pressure is limited by the available pressure in the gas bottle being coupled directly to the chamber [1].

Loading at 1500 bar hereby gives a calculated equilibrium concentration of molecular hydrogen in silica of 17.5 mole% at 21°C. This concentration is naturally a questionable value that needs to be verified through measurements, especially due to the predicted saturation of the equilibrium

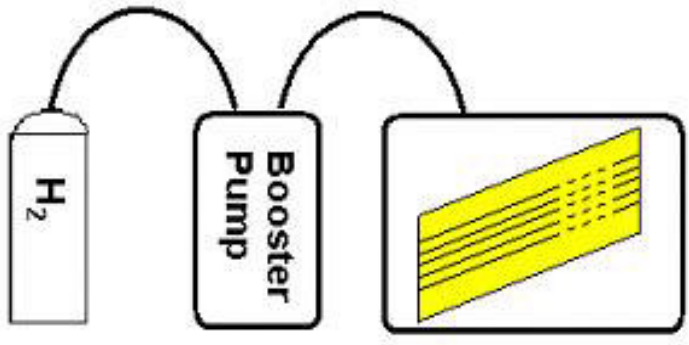

Figure 5-1: Schematic of the loading setup with the gas bottle supplying the booster pump, that pressurizes the contents in the chamber.

concentration [36][37].

5.2 Optical properties of loaded samples

In order to determine the concentration of molecular hydrogen dissolved in the core layer, a suitable measuring method, for planar waveguide samples, has to established. The Bragg grating method of estimating the concentration from the effective index shift is preferred, due to the short interaction length of typical planar waveguide structures (type 1). The method has previously been verified for optical fibers loaded at 110 bar [38]. However, we will verify the method for planar waveguide samples, by determining a correlation between the effective index drift and the absorption spectrum when loading up to a much higher pressure of 1500 bar.

5.2.1 Optical attenuation

The shape of the absorption spectrum for molecular hydrogen needs to be reviewed, as it is used as a reference for determining the concentration of hy-

Figure 5-2: Photograph of the high pressure loading system. The valves for controlling the pressure system is seen on the front plate, on top of the chamber, encapsulated by steel poles and the hydraulic system.

drogen dissolved in the germanosilica sample [35]. The hydrogen is assumed mainly to diffuse as interstitial molecules, without any interaction with the host glass network at room temperature [36] [45]. Otherwise, a product such reaction would be formation of OH groups [35], which though not is observed in absorption measurements for the present samples. Further measurements of the solubility (section 5.3.2) will support the assumption of hydrogen diffusing as molecules rather than as dissociated species.

Absorption spectrum

The hydrogen molecule is a symmetric diatomic molecule, hence it is optical transparent in gas phase. At high pressure, or when dissolved in a

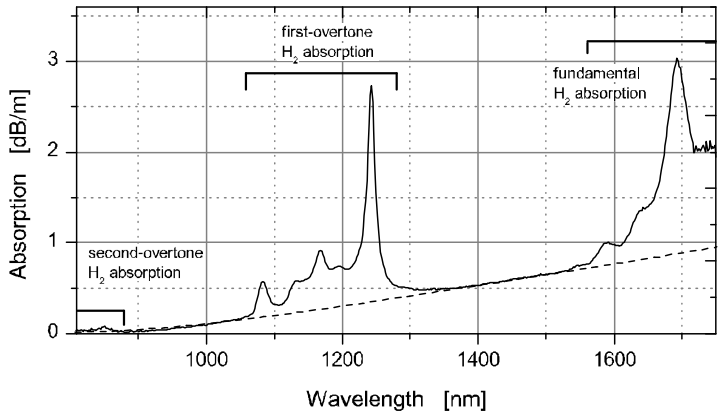

Figure 5-3: Absorption spectrum for hydrogen loaded fiber in the interval from 800 nm to 1750 nm, showing overtone absorption peaks and part of the fundamental absorption. (courtesy of M. Svalgaard)

solid, the symmetry is partially destroyed, leading to several absorption bands [46]. The fundamental absorption then consist of a strong resonance peak at a wavelength close to 2400 nm, with sidebands of lower absorption down to around 1500 nm. Figure 5-3 shows a measured absorption spectrum for a standard optical fiber, loaded with approximately 2.9 mole% of molecular hydrogen [1]. The absorption spectrum is found through transmission measurements, obtained with a broad band white light source and an optical spectrum analyzer (OSA). The figure clearly display some of the sidebands from the fundamental absorption, at wavelengths above 1550 nm and upto 1750 nm. The first overtone absorption bands are seen to be positioned between 1050-1350 nm, peaking at around 1245 nm with weaker sidebands at wavelengths down to 1080 nm. The weaker bands from the second overtone absorption are slightly visible around 850 nm. A broad off resonance absorption, that increases with wavelength, is indicated by a dashed line, starting close to 0 dB at 800 nm and crossing 0.7 dB/m at 1500

nm. Not having any significant OH induced absorption (typically peaking at wavelengths around 1400 nm), no other important loss mechanisms are expected [35]. Hence, after subtracting the off resonance absorption the concentration of molecular hydrogen, dissolved inside the waveguiding core region, can be estimated from the direct proportionality to the attenuation [35][45]. We are therefore confident that monitoring the attenuation at a wavelength of 1690 nm (part of the fundamental absorption band) is a valid measure for estimating the molecular hydrogen content in the following experiments.

The absorption band at 1690 nm is chosen since the other alternative is the overtone absorption bands, located at wavelengths where the present waveguide structures becomes multimoded. The absorption at 1690 nm is found from figure 5-3 to be 2.1 dB/m at a hydrogen concentration of 2.9 mole% [1], giving an attenuation of 0.72 dB/m per mole% of hydrogen dissolved. Determination of the molecular hydrogen concentration in the specific germanosilica samples are therefore found from measurements of the attenuation at 1690 nm, $\Delta\alpha_{1690nm}$, after off-resonance subtraction, according to the following expression:

$$[H_2](mole\%) = \frac{\Delta\alpha_{1690nm}[dB/m]}{0.72\frac{dB}{m}} \tag{5.2}$$

Consequently a hydrogen concentration of 17.5 mole% gives an absorption loss of 0.13 dB/cm at 1690 nm. Typical samples have waveguides of 3 cm length (type 1), corresponding to a hydrogen induced absorption loss of around 0.5 dB. During out-diffusion the absorption loss will decrease even further, so this type of measurements requires a longer interaction length. Planar waveguide structures folded to a total length of 110 cm on a 11 cm long sample (type 2), are therefore used to improve these measurements, giving an absorption loss of upto 15 dB.

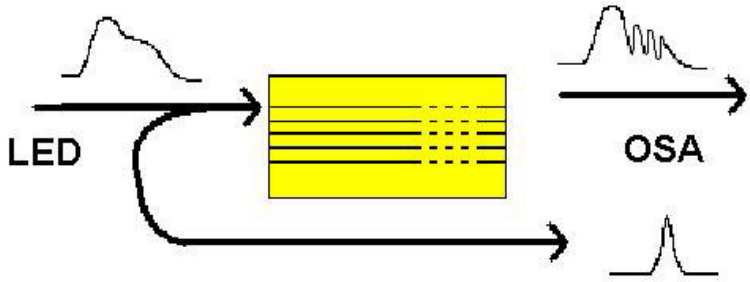

Figure 5-4: The measuring technique using an LED source and an OSA for obtaining absorption spectrum by transmission measurements, and the effective index from the Bragg reflection measurements.

5.2.2 Effective index drift

These planar waveguide samples of type 2 are used for correlating the effective index shift with the molecular hydrogen concentration after high pressure loading. The loading with molecular hydrogen is performed both at 820 and 1480 bar, lasting several weeks to ensure a saturation close to the equilibrium concentration.

These samples are hereafter placed on the fiber-optic characterization setup, where standard optical fibers are butt-coupled to both ends of the waveguide. A light emitting diode (LED) source is used to couple light through the specific waveguide and into the OSA, according to the two arrows going from left to right in the upper part of figure 5-4. The large intrinsic transmission loss of such folded waveguide structures, demands a high-power LED source. A typical measured absorption spectrum is seen on the small inset in the upper left corner of figure 5-5, showing a noisy 1690 nm absorption peak. From this a mean hydrogen induced attenuation is estimated, while the deviation between the estimated maximum and minimum attenuation gives a corresponding noise level. The Bragg resonance shift is measured in reflection immediately after each absorption

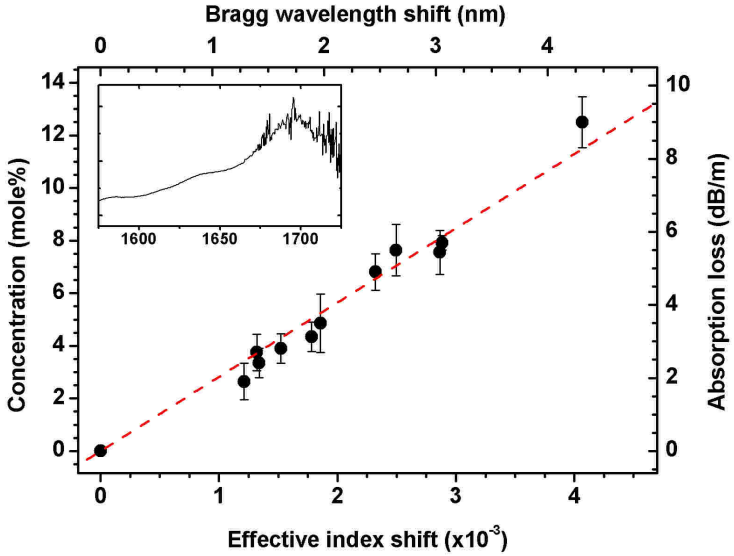

Figure 5-5: Plot of hydrogen concentration versus effective index shift, with the dashed line representing a linear fit to the measured data. The measurements are obtained from absorption measurements as shown in the small inset in upper left corner.

measurement, according to the curved arrow illustrated in the lower part of figure 5-4.

Such sets of measurements are acquired at different time intervals during a period of several days, while the hydrogen is allowed to diffuse out of the sample at a temperature of 23°C. The hydrogen concentration is plotted as a function of the calculated effective index drift by solid circles in figure 5-5, with error bars denoting the noise level. The hydrogen concentration is found from the measured attenuation (right axis) through equation 5.2, while the effective index is linked to the measured Bragg resonance (upper axis) by the Bragg condition (equation 2.2). As shown by the dashed line in figure 5-5 the measurements are well approximated by a linear fit, lying within the noise level of the measurements. The linear fit starts at origo,

and increases linearly towards a concentration of 11.5 mole% for an effective index shift of 4.1×10^{-3}. The slope of this fit indicate a concentration of 2.81 mole% for an effective index shift of 1×10^{-3}, or accordingly an index change of 0.024% per mole % molecular hydrogen dissolved.

We have hereby verified the linear correlation of the effective index shift upon the hydrogen content for planar germanosilica waveguide samples, loaded with molecular hydrogen upto around 12 mole%.

5.2.3 Birefringence

Visual microscope inspection of these high pressure loaded samples (type 2), showed macroscopic convex bending, that is reduced along with the out-diffusion of hydrogen. Such bending is typically seen in multilayer planar structures of different material, where uneven expansion coefficients causes stress build-up. In our case we expect the bending to be stress related, due to the diffusivity of hydrogen in silicon being several orders of magnitude larger compared to that of silica [47]. The silicon substrate is therefore assumed to be almost free of hydrogen after less than half an hour, while the silica still contains most of the initial concentration. The thick silicon substrate then prevents the silica thin-film from expanding in the horizontal plane, hereby causing a convex bending of the sample due to the compressive stress in the silica film. The hereby induced strain is directly proportional to the hydrostatic pressure from the presence of molecular hydrogen [48][49], so that the strain is reduced according to the hydrogen content in the silica film.

For an isotropic media, such as silica, the induced birefringence will be linear proportional to the strain during elastic deformation [50]. If the applied strain exceeds the regime of elastic deformation, a typical result would be bond-breaking or rupture of the silica material [49]. Several experiments of out-diffusion verified that the effective index, birefringence and absorption converged towards the initial values as was before loading. As no additional formation of OH groups are observed either, we assume not to have exceeded the elastic regime or having a reaction between the hydrogen

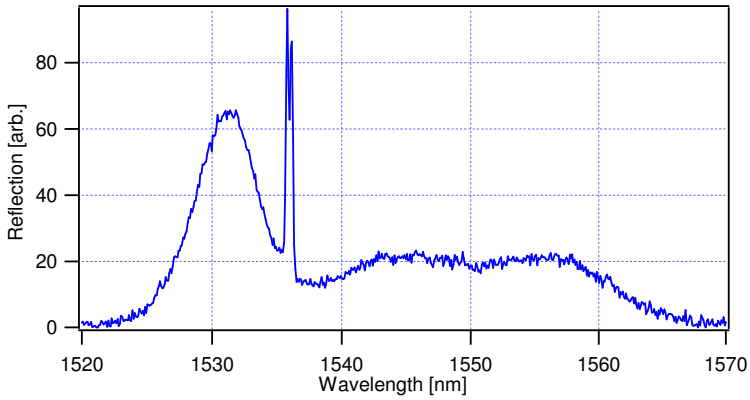

Figure 5-6: Reflection spectrum from high pressure loaded sample, showing both the broad ASE source reflection and the birefringent Bragg resonance peak.

and the silica network. Hence, the birefringence induced by high pressure hydrogen loading can be used as an additional parameter for determining the molecular hydrogen content.

Experimental

The birefringence ($n_{te} - n_{tm}$) is extracted from Bragg grating measurements performed according to figure 5-4, with the modification of the LED source being replaced by an unpolarized ASE source. A typical measured reflection spectrum is seen in figure 5-6 for a wavelength interval from 1520 to 1570 nm, showing narrow Bragg peaks centered around 1536 nm and a wide band emission spectrum from the ASE source probing the waveguide. This ASE reflection is part of the off-resonance transmission loss (section 5.2.1), which decreases as the hydrogen diffuses out of the sample.

A closer look at the Bragg resonance peak in figure 5-6 reveals polarization splitting of TE- and TM-polarized light, caused by the birefringence. Figure 5-7 shows the measured birefringence as a function of effective index

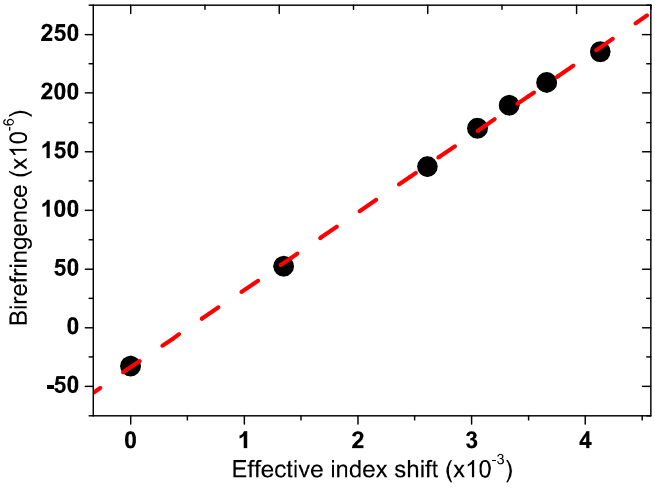

Figure 5-7: Birefringence as a function of effective index drift after high pressure hydrogen loading (solid circles), approximated by a linear fit (dashed line)

drift, with the birefringence being proportional to the content of molecular hydrogen. The data shows an intrinsic birefringence of around -30×10^{-6} before loading, that increases almost linear to 230×10^{-6} for an index shift of 4.1 nm (i.e. approximately 12 mole% of hydrogen) as indicated by the dashed line. This gives a dependence for the birefringence of 22×10^{-6} per mole% of molecular hydrogen dissolved in the specific sample. The linear behavior of the birefringence as a function of the effective index supports the conclusion of the effective index drift being proportional to the hydrogen content.

To summarize; we have verified, through measurements of the absorption and Bragg resonance, that the effective index drift, induced by loading with molecular hydrogen, is linear proportional to the concentration of

molecular hydrogen dissolved in the silica film. This correlation is observed to hold for concentrations up to at least 12 mole%, with an index proportionality factor of 0.024% per mole% of molecular hydrogen for these specific samples. Measurements of the birefringence, caused by the presence of interstitial hydrogen molecules, is found to vary as 22×10^{-6} per mole%. The linear dependence between the effective index drift and birefringence supports the Bragg grating method as being suitable for determining the concentration of molecular hydrogen in germanosilica thin film samples.

5.3 Diffusion and solubility in germanosilica

Having established the method for measuring the molecular hydrogen concentration in planar waveguide samples, we proceed to investigating the diffusivity and solubility in germanosilica. For a loading pressure around 1500 bar an equilibrium concentration of 17.5 mole% is predicted [2], which is somewhat larger than the 12 mole% measured only an hour after the sample was removed from the loading chamber. An explanation could be that the equilibrium concentration is saturated [36][37], or that the diffusion rate is larger than expected after loading at high pressures [9]. The diffusion rate is an important parameter for estimating the usable time before the loss of hydrogen/deuterium molecules will affect the UV-writing process [4], while the solubility is important for determining the obtainable equilibrium concentration for a given loading pressure. Hence, investigation of the diffusion behavior and solubility of molecular hydrogen in the specific high pressure loaded germanosilica samples will be conducted.

This section will describe experiments, where a Bragg grating is used to estimate the diffusion rate and solubility of hydrogen or deuterium in germanosilica thin-film samples. Even though the diffusivity of hydrogen is slightly larger compared to deuterium[45], the solubility of the two should be the same in silica [36].

5.3.1 Diffusion

The diffusion rate is found from continuously measuring the hydrogen content, during a long time period, in samples loaded under high pressure, while the hydrogen diffuses out of the sample at room temperature ($23°C$). In practice this is done by monitoring the effective index drift, according to the method described in section 5.2.2, and convert the measured index drift to a concentration of molecular hydrogen.

Diffusion equation

For the used samples (type 1) the 5.5 μm thick photosensitive germanosilica corelayer is sandwiched between two silica layers, with a cladding-layer thickness of 12 μm and a buffer-layer thickness of 16 μm. The corelayer extends over several thousand of μm in the horizontal plane, so the hydrogen will mainly diffuse out of the sample in a direction perpendicular to the buried corelayer. Without any reaction between hydrogen and silica such a one dimensional diffusion problem can be described by Ficks second law $\frac{\partial C(x,t)}{\partial t} = \frac{\partial}{\partial x} D \frac{\partial C(x,t)}{\partial x}$ [49]. Here D is the diffusivity of molecular hydrogen in silica, while $C(x,t)$ is the hydrogen concentration as a function of time, t, and position, x, below the surface. Assuming the three silica layers to be sufficient homogeneous, the diffusivity is considered everywhere constant. Since the diffusivity and solubility of hydrogen are orders of magnitude larger in silicon than silica [51], we can omit the silicon substrate material from the analysis and assume air instead. The problem is hereby reduced to molecular diffusion in an isolated silica thin-film, with the silica(buffer)/silicon(substrate) and air/silica(cladding) interfaces assumed to be saturated to the equilibrium concentration of the ambient atmosphere. Applying boundary conditions of a constant surface concentration, leads to a solution for diffusion through a single interface into a sample of infinite thickness of $C(x,t) = C_s \operatorname{erfc}(\frac{x}{2\sqrt{Dt}})$ [52]. Here erfc is the complementary error function and C_s the pressure dependent surface equilibrium concentration. As the dynamics for in- and out-diffusion are governed by the

Figure 5-8: Sketch of the three layer structure with x_1 denoting the vertical distance from the cladding/air interface to the waveguide center, and x_2 the distance from the buffer/substrate interface.

same diffusivity [53], we get a similar solution for the out-diffusion by substituting the complementary error function with an ordinary error function (erf $= 1 -$ erfc).

In our case the hydrogen diffuses in and out of the film from both sides, so the superposition principle is applied to the linear differential diffusion equation [52]. The equation describing the outdiffusion of molecular hydrogen from a homogeneously loaded thin film hereby becomes:

$$C(x,t) = C_{s1}\,\mathrm{erf}(\frac{x_1}{2\sqrt{Dt}})) + C_{s2}\,\mathrm{erf}(\frac{x_2}{2\sqrt{Dt}})) \tag{5.3}$$

The first term on the right hand side describes diffusion through the cladding side, and the second term diffusion through the substrate/buffer at the opposite side. The constant x_1 denotes the total vertical distance from the cladding/air interface to the waveguide center, while x_2 denotes the distance from the buffer/substrate interface according to figure 5-8. Applying boundary conditions for $t \to \infty$ gives the surface concentration on both sides of the thin film equal to one half of the surface concentration ($C_{s1} = C_{s2} = C_s/2$).

This approximation of the thin film diffusion with an expression based on diffusion in samples of infinite thickness, may cause errors. For instance, we use a surface concentration on each side, which only is one half of the

actual surface concentration, while the case should be that $C_{s1} = C_{s2} = C_s$. Thus, using the expression $C(x,t) = C_s \operatorname{erfc}(\frac{x}{2\sqrt{Dt}}))$ for describing in diffusion through one side may be a better estimate of the actual loading process. Another effect, not taken into account, is the concentration gradient across the waveguide region, and the power profile of the probe light guided through the waveguide [44]. It may prove possible to find better solutions using simulation tools or other analytical expressions, but for the purpose of giving a quick estimate of the molecular hydrogen concentration during out-diffusion the following section will show the expression given in equation 5.3 to be adequate for samples loaded at a pressure of 190 bar.

Experimental

A sample (type 1) is loaded with deuterium under a pressure of 190 bar at 3°C for several months, and then stored at -130°C for several years. The sample is afterwards placed on the characterization setup, whereby the deuterium content is measured for a period of more than 25 hours, according to section 5.2.2. From these measurements, conducted at a temperature of $23°C$, we obtain the deuterium concentration as a function of time, as shown by the hollow circles in figure 5-9. The measured deuterium content in the core region is hereby seen to decrease smoothly from around 2.95 to 1.6 mole% during a time interval starting at 50 minutes and going to more than 1500 minutes (the step like behavior is caused by quantization errors).

Given a diffusivity of $1.4 \times 10^{-11}\ cm^2/s$ we find an approximative fit to this concentration curve using equation 5.3, as shown by the dashed line in figure 5-9. The fitting parameters used are a surface concentration of $C_s = 3.05\ mole\%$, a waveguide distance from the cladding/air interface of $x_1 = 8\ \mu m$ and from the cladding/air interface of $x_2 = 17\ \mu m$. Hereby the expression of equation 5.3 seems to fit the measured data quite well. These values of x_1 and x_2 does not reflect the actual distance to the center of the core, but rather the distance to the corelayer interface. This could be a result of the surface concentration (C_{s1} and C_{s2}) only being one half of the actual (C_s).

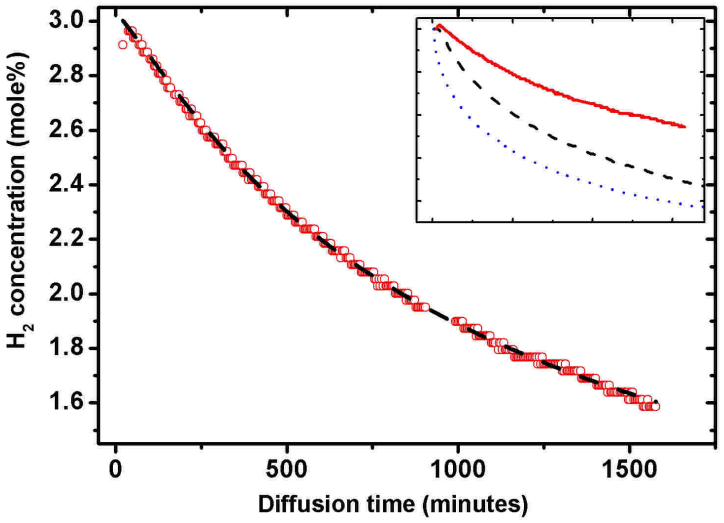

Figure 5-9: Hydrogen concentration during out diffusion for sample loaded under a pressure of 190 bar at 3°C. The small inset are normalized curves for samples loaded at different pressures, showing different diffusion rates.

Similar measurements of the concentration as a function of time are conducted for samples loaded with molecular hydrogen at 190, 500 and 1480 bar, as shown by the curves in the small inset of figure 5-9. These curves are normalized with respect to the measured start concentration, obtained as fast as possible after removing the samples from the loading chamber. The solid line corresponds to measurements from the sample loaded at 190 bar (3°C). The dashed line is from measuring the hydrogen content after loading at 500 bar (18°C), while the dotted line is from loading at 1480 bar (21°C).

An important notice to this figure is that the curves are seen to exhibit different decay rates depending on the loading pressure. We observe a faster diffusion in a sample loaded at 1480 bar compared to the same sample

loaded at 190 bar. The curve for a sample loaded at 500 bar is located in between these two. Equation 5.3 is not capable of describing the measured data for all of these three experiments with the given parameters. This diffusion behaviour could be due to an additional driving force or increased diffusivity, enhancing the diffusion rate [49] dependent on the concentration of hydrogen molecules in the sample. The same observation of an increased diffusion rate depending on the loading pressure is observed in experiments with optical fibers loaded at upto 2000 bar [9]. So in order to estimate the molecular hydrogen content in high-pressure loaded samples (>200 bar), experimental determined values will be used instead of an expression similar to that of equation 5.3. Experiments of loading with deuterium instead of hydrogen produced similar results, though the diffusion rate is somewhat lower [45].

Waveguide fabrication by the Direct UV writing method is typically performed in less than 24 hours, during which the sample temperature is around -35°C. This gives a corresponding time scale at room temperature of less than half an hour. According to figure 5-9 a sample containing around 3 mole% of hydrogen will loose less than 3% of this during a 24 hour time interval. Relating this to the waveguide fabrication process of direct UV writing, the index step of such fabricated waveguides will decrease by approximately 6×10^{-4} (chapter 3), if none of the writing parameters (0.6 MW/cm^2 and scan velocity of 200 $\mu m/s$) are changed during this interval. However, considering fabrication of waveguides in samples containing 17.5 mole% of hydrogen, the increased diffusion rate causes a concentration decrease of 15% to around 14.9 mole%. The corresponding index for waveguides fabricated (using an UV intensity of 0.3 MW/cm^2 and a scan velocity of 300 $\mu m/s$) will hereby decrease by 1×10^{-3}, a significant index difference that will have to be taken into account. These values are based on the waveguide fabrication process being performed with writing parameters optimized for the present concentration range, so UV intensity and scan velocity is quite different for the two cases.

5.3.2 Solubility

Estimation of the equilibrium concentration of molecular hydrogen in the specific germanosilica samples after high pressure loading is another important parameter, in order to determine a suitable UV power and scan velocity range for UV writing.

The calculation of the equilibrium concentration depends on the solubility, S, according to equation 5.1. In general the solubility, S, is related to the diffusivity, D, and permeability, K, as $K = DS$ [42]. The solubility can be expressed in a typical Arrhenius form $S = S_0 \exp(\frac{-E_s}{kT})$, where S_0 is the solubility constant, E_s the enthalphy, T the absolute temperature and k the Boltzmann factor. The temperature dependence of the solubility have not been studied, thus we rely on values for the enthalphy, E_s, from similar experiments with optical fibers [2][35].

Due to a possible existence of a saturation effect, limiting the amount of hydrogen that can be dissolved into silica [36][37], we will experimentally investigate the solubility of molecular hydrogen in the specific germanosilica samples. Determination of the solubility is based on measuring the concentration of hydrogen immediately after the samples are removed from the loading chamber, according to the method described in section 5.2.2.

Experimental

The equilibrium concentration of dissolved hydrogen immediately after ending the loading process, is determined from the concentration curves, according to section 5.3.1, for planar waveguides samples of type 1.

Samples are loaded for at least 18 days, whereby we expect a saturation to more than 95% of the equilibrium concentration [1] (equation 5.3 is not usable due to the diffusion behaviour discussed in section 5.3.1). Since the solubility depends on temperature, the corresponding loading pressure for samples loaded at different temperatures (between 3°C and 23°C) are converted to a loading pressure that would result in the same equilibrium concentration, but at a loading temperature of 21°C. This is done according

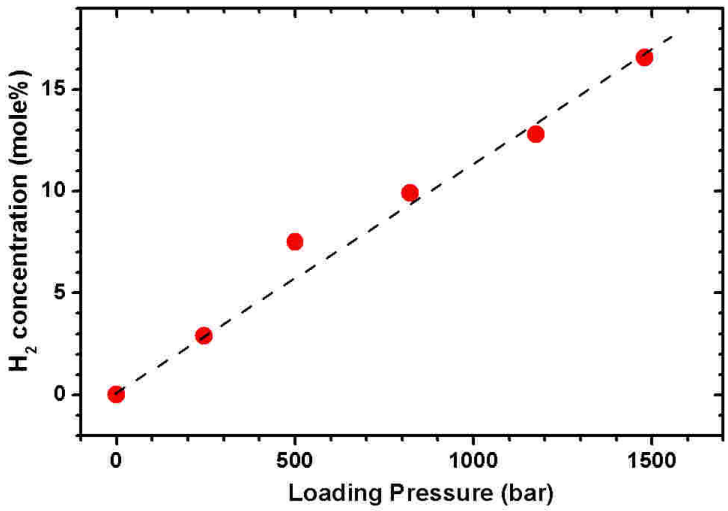

Figure 5-10: Measured equilibrium concentration of hydrogen dissolved in samples as a function of loading pressure (solid circles), approximated by a linear fit (dashed line)

to the proportionality factor of exp(8.67kJ/mole/RT), so that the pressure used in figure 5-10 corresponds to all samples being loaded at 21°C. Due to difficulties of coupling light into samples loaded at 1480 bar within the first hour, the equilibrium concentration for these have been obtained by extrapolation of the diffusion curve.

The measured equilibrium concentration of molecular hydrogen as a function of loading pressure is seen on figure 5-10, starting at origo and increasing almost linear upto a pressure of 1500 bar. The dashed line shows a linear fit to the measured data, with a slope of 11.2×10^{-3} mole%/bar (112 ppm/bar) at 21°C. No saturation effect is observed for the analyzed pressure range from 0 to 1500 bar. Samples have been loaded at pressures upto 1800 bar, but so far it has been impossible to couple light into these

waveguides during the first hour. So it seems that this method of using a waveguide to guide the probe light is limited to experiments in samples having molecular hydrogen contents of less than 16 mole% (loading pressure below 1500 bar). Consequently we conclude the solubility of molecular hydrogen in the specific silica thin-film samples to be constant in the loading range upto 1500 bar (16 mole%) with the value of $S = 112\frac{ppm}{bar}$.

We have hereby shown the solubility to be concentration independent with a value of $112\frac{ppm}{bar}$ at a temperature of 21°C, which is close to the previous result of $116\frac{ppm}{bar}$ obtained from experiments using optical fibers [35]. For the present samples the equilibrium concentration of hydrogen does not seem to saturate in a loading pressure range from 0 to 1480 bar (concentration range from 0 to 16 mole%). However, the diffusivity is seen to depend on the hydrogen concentration after high pressure loading, which could be caused by additional driving forces 'pushing' the molecules out of the material. This effect might be connected to the density of hydrogen molecules dissolved in the samples being comparable to the density of silica interstices [36][37]. Hence, one might expect an increase of the time required for loading to a high molecular concentration. However, the performed experiments only deals with out diffusion, so we have not been able to investigate the high pressure loading process in details. An important note to figure 5-10 is the linear dependence of the measured concentration on loading pressure, which indicates a molecular rather than a dissociative solubility [34]. This support the assumption of the hydrogen diffusing as molecules in silica, and hence the molecules being dissolved in silica intestices.

Chapter 6

Conclusion

During my Ph.D. project, I have been concerned about investigating several fundamental aspects of the direct UV-writing technique, by which optical waveguide structures are formed in hydrogen or deuterium loaded planar germanosilica glass. The photosensitivity of such samples is found to increase along with the hydrogen or deuterium content. For this reason a high pressure loading system has been implemented, by which we are capable of loading samples at a pressure of almost 2000 bar. Experiments of fabricating waveguides in such high pressure loaded samples have though shown some unexpected effects, which are believed to be of fundamental interest for the direct UV writing process. Effects that have been investigated in detail for the specific samples, by luminescence spectroscopy, thermal annealing and studies of the behavior of molecular hydrogen after high pressure loading. The main conclusions of this work is summarized in the following.

UV writing setup: The important parts of the Direct UV-writing setup, used during the fabrication of optical waveguide structures in planar germanosilica samples, are described. The key elements of this setup are the 257 nm gas laser source, the beamshaping elements, translation stages and the germanosilica samples in which waveguides are formed. The beam characteristics of the setup is measured, by which a spotsize of 3 μm di-

ameter is found. The characterization setup and the related methods for characterizing the fabricated waveguide structures are described briefly.

UV written waveguides: Optical waveguides are fabricated in germanosilica samples with this UV writing setup, after loading with molecular hydrogen up to 20 mole%. Using an average UV intensity of 0.3 MW/cm^2, while allowing the hydrogen diffuse out of the sample, shows an UV induced refractive index change that decrease along with the hydrogen concentration by 0.6×10^{-3} per mole%. Several discontinuous points are observed at 12, 14 and 16.5 mole%, where the resulting UV induced refractive index change exhibits a step like behavior. A similar behavior is not observed while using an UV intensity of 0.7 MW/cm^2 and similar samples loaded with only 3 mole%. These steps are believed to be a physical effect of the hydrogen concentration changing, and might be related to transfer of energy from specific sites in the surrounding glass matrix during the UV exposure.

Similar abrupt index changes are observed for waveguides fabricated with various scanning velocities, indicating the existence of some kind of threshold. Varying the scanning velocity, while fabricating waveguides in samples loaded to 20 mole% with an incident UV intensity of 0.3 MW/cm^2, causes a sudden drop in the induced refractive index change after exceeding scanning velocities in excess of 600 μm/s.

Further experimental optimization results in a UV induced refractive index change of upto 19×10^{-3}, obtained with samples loaded to 20 mole% of hydrogen and after exposure with an UV intensity of 0.5 MW/cm^2. The obtainable UV induced index change is limited by the damage inflicted upon the samples during the UV exposure. This limit is found to be around 1 MW/cm^2 for samples loaded with 3 mole% of hydrogen at a given scan velocity, but drops to only 0.5 MW/cm^2 for samples loaded with 20 mole%.

A problem related to the fabrication of splitter and coupler structures by direct UV writing is investigated. The problem arise during fabrication of closely spaced waveguides, which are found to suffer from an index asymmetry. A method to correct for the induced asymmetry is applied

during fabrication of such devices, whereby reliable symmetric devices are obtained. From subsequent experiments it is concluded that the asymmetry most likely is caused by deuterium diffusion, due to local heating induced by the high intensity UV beam.

UV induced defects in germanosilica: The observed threshold effect is investigated through photoluminescence spectroscopic measurements of samples, treated by UV exposure at different intensities and heating to $400°C$. From these measurements it is found that the observed increase of the blue luminescence, seen to accompany the initiation of the UV induced index change, not is caused by an increased concentration of the twofold coordinated germanium defect center (GODC). It is proposed that the sudden enhancement of the blue luminescence is caused by a temperature increase, from absorption of UV photons by such GODC's. Hence, the threshold is not caused by different a concentration of the particular twofold coordinated germanium centers. Neither does rapid heating to $400°C$ cause a significant increase in number of this specific GODC, a fact supported by flamebrushing experiments with similar samples.

The thermal stability of the UV induced refractive index change is investigated by thermal annealing of UV written waveguides. The index decay is modelled by a previously known electron trap model, whereby a bell shaped index distribution is found to be centered around a demarcation energy of 2.1 eV. It is estimated that the UV induced refractive index change only decay around 0.7 % during the first 25 years of normal operation at $25°C$, when a post-process annealing at $80°C$ for 24 hours is performed.

Molecular hydrogen in silica thin-films: A suitable method for measuring the concentration of molecular hydrogen in planar germanosilica waveguide samples is verified for concentrations up to 12 mole%. The method make use of a Bragg grating to monitor the effective index drift and birefringence. The effective index drift is found to be 0.024% per mole%, while the birefringence change by 21×10^{-6} per mole%.

This method is successfully used to estimate the hydrogen or deuterium concentration prior to UV exposure. An approximative model is applied,

by which we are able to calculate the hydrogen concentration for samples loaded at a pressure below 200 bar (3 mole%). The diffusivity of molecular hydrogen is seen to depend on the concentration, causing an increased diffusivity at high concentrations. The solubility of molecular hydrogen in germanosilica samples is found to be independent on the concentration, with an equilibrium concentration proportional to the loading pressure; measured as $112\frac{ppm}{bar}$ at a temperature of 21°C. This relation is proven valid in the range from 0 to 16mole%, with no indication of saturation.

Bibliography

[1] M. Svalgaard, *Ultraviolet light induced refractive index structures in germanosilica*. PhD thesis, Mikroelektronik centret, DTU, 1997.

[2] P. J. Lemaire, R. M. Atkins, V. Mizrahi, and W. A. Reed, "High pressure H2 loading as a technique for achieving ultrahigh UV photosensitivity and thermal sensitivity in GeO2-doped optical fibres," *Electronic Letters* **29**(13), pp. 1191–1193, 1993.

[3] K.Færch, "Direct UV-written waveguides," Master's thesis, COM center,DTU, 2000.

[4] M. Svalgaard, "Effect of deuterium outdiffusion on direct UV writing of optical waveguides," *Electronic Letters* **35**(21), 1999.

[5] Coherent, *Modemaster Beam Propagation Analyzer*.

[6] A. Harpøth, "Advanced characterization methods of UV-written waveguides," Master's thesis, COM center, DTU, 2001.

[7] K. O. Hill, B. Malo, F. Bilodeau, D. C. Johnson, and J. Albert, "Bragg gratings fabricated in monomode photosensitive optical fiber by UV exposure through a phase mask," *Applied Physical Letters* **62**(10), pp. 1035–1037, 1993.

[8] M. Kristensen, "Ultraviolet-light-induced processes in germanium-doped silica," *Phys. Rev. B* **64**, pp. 144–201, 2001.

[9] J. Brennan, "The photosensitivity and UV-induced optical loss of silica optical fibers exposed to very high-pressure hydrogen environments," *SPIE, OFC* **3847**, pp. 42–47, 1999.

[10] J. Bernardin and N. Lawandy, "Dynamics of the formation of bragg gratings in germanosilicate optical fibers," *Opt. Communication* **79**, p. 194, 1990.

[11] D. Hand and P. Russel, "Photoinduced refractive index changes in germanosilicate optical fibers," *Opt. Lett.* **15**, pp. 102–104, 1990.

[12] M. Douay, W. Xie, T. Taunay, P. Bernage, P. Niay, P. Cordier, B. Poumellec, L. Dong, J. Bayon, H. Poignant, and E. Delevaque, "Densification involved in the UV based photosensitivity of silica glasses and optical fibers," *Journal of Lightwave Technology* **15**, pp. 1329–1342, 1997.

[13] R. Loudon, *The Quantum Theory of Light*, Oxford university press, London, 1973.

[14] G. Pacchioni, L. Skuja, and D. L. Griscom, *Defects in SiO2 and Related Dielectrics: Science and Technology*, Kluwer Academic Publishers, Dordrecht-Boston-London, 2000.

[15] B. Poumellec, M. Douay, J. Krupa, J. Garapon, and P. Niay, "Comparison of UV optical absorption and UV excited luminescence behaviours in ge doped silica under h2 loading or CW UV laser irradiation," *Journal of non-crystalline solids* **317**, pp. 319–334, 2003.

[16] R. Atkins, P. Lemaire, T. Erdogan, and V. Mizrahi, "Mechanisms of enhanced UV photosensitivity via hydrogen loading in germanosilicate glasses," *Elec. Lett.* **29**, pp. 1234–1235, 1993.

[17] J.Hübner, *Index Engineering with Excimer Light.* PhD thesis, Mikroelektronik centret, DTU, 1998.

[18] D. Zauner, K. Kulstad, J. Rathje, and M. Svalgaard, "Directly UV-written silica-on-silicon planar waveguide with low insertion loss," *Electronic Letters* **34**(16), pp. 1582–1584, 1998.

[19] M. Yuen, "Ultraviolet absorption studies of germanium silicate glasses," *Appl. Optics* **21**, pp. 136–140, 1982.

[20] L. Skuja, A. Trukhin, and A. Plaudis, "Luminescence in germanium-doped glassy SiO2," *Phys. Stat. Sol. (a)* **84**, pp. 153–157, 1984.

[21] A. Sakoh, M. Takahashi, T. Yoko, J. Nishi, H. Nishiyama, and I. Miyamoto, "Photochemical process of divalent germanium responsible for photorefractive index change in GeO2-SiO2 glasses," *Optics Express* **11**, pp. 2679–2687, 2003.

[22] A. Iino, M. Kuwabara, and K. Kokura, "Mechanisms of hydrogen-induced losses in silica-based optical fibers," *Journal of Lightwave Technology* **8**, pp. 1675–1679, 1990.

[23] H. Kuswanto, F. Goutaland, A. Yaha, A. Boukenter, and Y. Querdane, "Temperature, h2 loading and ultra violet irradiation effects in germanosilicate optical fibers: Laser spectroscopy measurements," *Journal of non-crystalline solids* **280**, pp. 277–280, 2001.

[24] K. Awazu, H. Kawazoe, and M. Yamane, "Simultaneous generation of optical absorption bands at 5.14 and 0.452 eV in 9 SiO2:GeO2 glasses heated under an h2 atmosphere," *J. Appl. Phys.* **68**, pp. 2713–2718, 1990.

[25] M. Fokine and W. Margulis, "Large increase in photosensitivity through massive hydroxyl formation," *Optic letters* **25**, pp. 302–304, 2000.

[26] V. Volkov, "The luminescence of cluster derivatives of boron hydrides and some applied aspects," *Chemistry for sustainable development* **8**, pp. 185–191, 2000.

[27] J. R. Lakowicz, *Principles of Fluorescence Spectroscopy*, Plenum Press, New York and London, 1983.

[28] M. Andersen, "Direkt UV-skrivning af bølgeledere med udvidede egenskaber," Master's thesis, COM center, DTU, 2003.

[29] T. Erdogan, V. Mizrahi, P. Lemaire, and D. Monroe, "Decay of ultraviolet-induced fiber bragg gratings," *Journal of Applied Physics* **76**, pp. 73–80, 1994.

[30] K. Chisholm, K. Sugden, and I. Bennion, "Effects of thermal annealing on bragg fibre gratings in boron/germania co-doped fibre," *Applied Physics* **31**, pp. 61–64, 1998.

[31] J. Rathje, *Thermal Stability and Practical Applications of UV Induced Index Changes in Silica Glasses*. PhD thesis, COM center, DTU, 2000.

[32] G. Robert and I. Riant, "Demonstration of two distributions of defect centers in hydrogen-loaded high germanium content fibers," *OFC Technical Digest* , pp. 180–181, 1997.

[33] H. R. Sørensen, "UV-written advanced bragg gratings in optical waveguides using a 266 nm cw laser," Master's thesis, COM center, DTU, 2003.

[34] J. Shackelford, P. Studt, and R. Fulrath, "Solubility of Gases in Glass. II. He, Ne, and H2 in Fused Silica," *Appl. Phys.* **43**, pp. 1619–1626, 1972.

[35] P. Lemaire, "Reliability of optical fibers exposed to hydrogen: Prediction of long-term loss increase," *Optical engineering* **30**, pp. 780–789, 1991.

[36] J. Shelby, "Molecular diffusion and solubility of hydrogen isotopes in vitreous silica," *Journal of Apllied physics* **48**, pp. 3387–3394, 1977.

[37] C. Hartwig, "Raman scattering from hydrogen and deuterium dissolved in silica as a function of pressure," *Journal of applied physics* **47**, pp. 956–959, 1976.

[38] P. Swart and A. A. Chtcherbakov, "Study of hydrogen diffusion in Boron/germanium codoped optical fiber," *Journal of lightwave technology* **20**, pp. 1933–1941, 2002.

[39] J. Brennan, "The behaviour of silica optical fibers expposed very high-pressure hydrogen environments," *Technical digest OFC/IOOC* **3**, pp. 59–61, 1999.

[40] B. Malo, J. Albert, K. Hill, F. Bilodeau, and D. Johnson, "Effective index drift from molecular hydrogen diffusion in hydrogen-loaded optical fibers and its efect on bragg grating fabrication," *Elec. Lett.* **30**, pp. 442–444, 1994.

[41] R. Syms and J. Cozens, *Integrated Optics*, Mcgraw-Hill, Berkshire, England, 1997.

[42] J. Shackelford, "Gas solubility in glasses - principles and structural implications," *Journal of non-crystalline solids* **253**, pp. 231–241, 1999.

[43] J. Stone, A. Chraplyvy, and C. Burrus, "Gas-in-glass- -a new raman gain medium: Molecular hydrogen in solid-silica optical fibers," *Optic Letters* **7**, pp. 297–299, 1982.

[44] A. Marshall, J. Irven, and N. Pitt, "Hydrogen and deuterium gas-in-glass effects in single-mode optical fibres," *IEE proceedings* **132**, pp. 172–176, 1985.

[45] J. Stone, "Interactions of hydrogen and deuterium with silica optical fiber: A review," *Journal of Lightwave technology* **5**, pp. 712–733, 1987.

[46] J. Stone, A. R. Chraplyvy, J. M. Wiesenfeld, and C. A. Burrus, "Overtone absorption and raman spectra of H2 and D2 in silica optical

fibers," *ATT Bell Laboratories Technical Journal* **63**, pp. 991–1000, 1984.

[47] G.Panzarini and L. Colombo, "Hydrogen diffusion in silicon from tight-binding molecular dynamics," *Physical Review letters* **73**, pp. 1636–1639, 1994.

[48] K. Chiang, "Pressure-induced birefringence in a coated highly birefrigent optical fiber," *Journal of Lightwave Technology* **8**, pp. 1850–1855, 1990.

[49] S. Elliot, *The Physics and Chemistry of Solids*, John-Wiley, 2000.

[50] M.Born and E. Wolf, *Principle of Optics*, Cambridge University Press, 1999.

[51] M. Binns, S. Mcquaid, R. Newman, and E. Lightowlers, "Hydrogen solubility in silicon and hydrogen defects present after quenching," *Semiconductor science and technology.* **8**, pp. 1908–1911, 1993.

[52] A. Grove, *Physics and Technology of Semiconductor Devices*, John-Wiley, New York, 1967.

[53] R. Lee, "Diffusion of hydrogen and deuterium in fused quartz," *Journal of chemical physics* **36**, pp. 1062–1071, 1962.